Heterogeneous axonal delay improves the spiking activity propagation on a toroidal network

DOCTOR OF PHILOSOPHY

Author: Salustri Marcello

(215301)

Supervisor: Professor Micheletto Ruggero

Department of Physics

College of Nanoscience

YOKOHAMA CITY UNIVERSITY

Yokohama, Kanazawa-ku, Seto, 22-2, Japan

Postal code:236-0027

Year: 2024

Contents

General Introduction

Background

The study of neural network systems in the brain has gained increasing importance over the past few decades. Human cognition and behavior are governed by the brain's neural network system. Analyzing this system can provide insight into how information is processed and decisions are made. Based on the brain's neural network system, artificial neural networks (ANNs) have been developed as a key component of artificial intelligence (AI) systems [1]. Scientists can gain insight into information processing, learning, and adaptation by studying biological neural networks. A greater understanding of these insights will enable ANN design and optimization to be more precise, resulting in more sophisticated artificial intelligence systems, and promoting advancements in technology and robotics. Neurological networks in the brain have remarkable capabilities, including pattern recognition, sensory integration, motor control, and adaptive learning [2]. Researchers and engineers have gained a deeper understanding of how the brain works through the study of its neural network system [3]. The emergence of these powerful algorithms has enabled the development of robotic systems and machine learning algorithms capable of recognizing patterns, integrating sensory information, and learning from their surroundings [4]. It is in this scenario that stochastic resonance (SR) plays a critical role. SR is a phenomenon that occurs in nonlinear systems, including neural networks, where noise can enhance the transmission of signals [5]. In the context of neural network spiking activity, stochastic resonance refers to the idea that noise in the system can improve the network's information processing capabilities [6]. Neural networks are made up of interconnected neurons that communicate via electrical signals or spikes. The generation and propagation of these spikes are influenced by various factors, including input signals and structural properties of individual neurons [7]. The introduction of noise into a neural network can have different effects depending on the system-specific properties. Stochastic Resonance adjusts the noise floor to optimize network performance. When the noise is at an optimal level, it can improve the network's response to weak input signals that would otherwise be undetectable or difficult to distinguish from background activity [8]. Stochastic resonance in the peak activity of neural networks has been extensively studied to understand its impact on information processing in the brain. It has been hypothesized that noise can enhance signal recognition, enhance the presentation and transmission of sensory information, and even affect decision-making [9]. Researchers have studied the mechanisms underlying stochastic resonance in neural networks and have proposed various theoretical models to explain [10] its occurrence. These models often involve complex interactions between the network architecture, the properties of individual neurons, and the properties of input signals and noise [11]. Experimental studies have provided evidence of stochastic resonance in neural systems [12]. These studies aim to better understand how stochastic resonance affects neural coding and information processing. Overall, the stochastic resonance in the peak activity of neural networks illustrates the complex relationship between noise and information processing in the brain. By understanding the principles underlying stochastic resonance, researchers

hope to unravel the complex dynamics of biological systems. They may develop novel strategies to improve information processing in artificial neural networks or to treat certain neurological diseases. To study the impact of noise on neural system function, we employ a novel approach in which we mimic the role of noise through the incorporation of axonal and neural heterogeneity. Axonal heterogeneity refers to the variability in the physical characteristics of neuronal axons, such as differences in axon diameter or myelination. Neural heterogeneity, on the other hand, encompasses the diversity in neural properties, such as neuronal excitability, firing thresholds, and synaptic strengths, within a neural population. By introducing axonal and neural heterogeneity into our modeling framework, we effectively emulate the impact of noise on neural network behavior. This approach allows us to investigate how the inherent variability in axonal and neural properties can influence the overall dynamics, stability, and information-processing capabilities of neural circuits. Furthermore, our work sheds light on the potential functional advantages and robustness that might be conferred by such heterogeneity in the presence of noise, thereby contributing to a deeper understanding of the role of variability in neural systems.

Motivation for the present research work

It is undeniable that the human brain consists of an incredibly complex biological neural network system capable of performing a wide variety of calculations. Since the brain contains approximately 86 billion neurons and 85 billion non-neuronal cells, the heterogeneity of these cells reveals several physiological rhythms that affect its function [13]. This cell diversity enables the brain to process and store information in unique ways, which allows a wide range of cognitive abilities to unfold. This complexity allows the brain to adapt to new situations, change its organization, and maintain its plasticity. By exploiting these properties, scientists have begun to apply the principles of neural networks to design artificial intelligence systems. Modern neuroscience is concerned with the extensive development of mathematical models that describe the biological workings of dynamic systems that resemble the brain. Because of the large amount of brain-related data collected over time, there has been a proportional preoccupation with mathematical computer simulations and comparing them with experimental results [14]. From a larger perspective, the brain is a complex system whose signaling takes place in a noisy heterogeneous environment [15]. In modern neuroscience, the considerable development of mathematical models has facilitated the realization of dynamic systems that resemble the biological functioning of the brain [16]. Among such studies, stochastic resonance, a counterintuitive mechanism by which embedded noise [17] increases a system's sensitivity and enhances its performance at a finite level, is believed to play an active role in a variety of classes of both natural phenomena and artificially structured neural systems [18]. Several studies show how stochastic resonance produces significant improvements in signal detection [19]. In this study, we aim to contribute to this area by investigating how the combination of axonal and neural heterogeneity enhances spike propagation in an ANN. We also want to find a simple mathematical model that explains the mechanism by which heterogeneity [20] can enhance signal propagation within neurons. Notable examples include studies on transcranial random noise stimulation (tRNS), in which subjects are stimulated by large electrodes with weak ran-

dom electrical stimuli that actually improve their various motor, sensory, and even cognitive tasks [21]. Given the brain's heterogeneity, [15], we investigated the nature and effects of two types of heterogeneity with the realistic neural model using the pyNest simulator on a toroidal network. The initial source of heterogeneity pertains to the diversity in axonal delay, which reflects the spatial separation between neurons. The second source of heterogeneity concerns the variability in the dynamic characteristics of neurons. In a real brain, neurons are not arranged in a regular grid-like in a crystalline structure. Instead, their position is affected by randomness. Since in a model network, the distance between neurons is represented by the propagation delay, in this study we determine how the increase of axonal heterogeneity reduces the time delay of signaling within a simple ANN. In particular, we use the Izhikevich neuron model implemented on a toroidal network [17, 22] to study the different time delays of a signal traveling through the network. We manipulate the system to achieve different levels of heterogeneity by axonal delay manipulation. Heterogeneity was implemented using a uniformly distributed parameter. Neurons in the brain process information in limited areas that generally have no defined ends or boundaries. In this sense, choosing a torus rather than a bounding layer or plane is natural because of its boundless nature. The use of the toroidal topology in previous studies [23] together with the mathematical topological nature of the torus, which we might want to use for future research, led us to design our network in a ring shape. We find that the increase in axonal heterogeneity corresponds to a decrease in the propagation time of the information. This is done from an input defined as *initiator* n_{in} to an arbitrary test neuron named *output* n_o. Communication between neurons occurs via action potentials (spikes), which travel to neighboring neurons and trigger other spikes. Overall, this creates a wave of spikes that propagate through the network. In addition, as numerous studies, [24–27], emphasize the utility of entropy in neuroscience, this research proposes a model that links axonal and neuron heterogeneity with interspike train entropy, leveraging the algebraic concept of equivalence classes to categorize brain entropy into distinct sets. This division into subsets simplifies both theoretical and computational investigations. The model's objective is to streamline the analysis of information within neural networks by grouping numerous brain cells into sets based on their equivalence class.

Neuron model

Introduced in 1952 and awarded the Nobel Prize in 1963, the Hodgkin-Huxley model uses large-scale nonlinear differential equations [28] to mathematically describe all plausible action potential patterns and biological membrane properties. Over the years, models have been developed for more complex systems. A remarkable implementation of the Hodgkin-Huxley model was published by Eugene M. Izhikevich [29]. He combines the biological results of his model with the integration and firing of neurons in his two-dimensional system of ordinary differential equations. Izhikevich program reproduces about 20 different responses that characterize real neurons' spiking behavior. The model's toroidal structure emulates a finite neural domain. Specifically, each node is connected to the nearest node, and the corresponding nodes on the opposite edge are circularly connected. Communication between each node, in a 2D grid, can be done in the following four directions: +x or east, -x or west, +y or north, -y or south. A torus network

can be defined as a graph $G = (N, C)$. Where $N(G)$ and $C(G)$ are the nodes and connections of G [30]. The total number of nodes in a 2D torus is n^2, and a 2D torus structure naturally leads to a von Neumann neighborhood. The simulation is started by choosing a neuron (corresponding to a node in the ring network) to act as a stimulus. This is called *initiator*, indicated with n_i. It is connected to a constant external current of $I = 10mA$ which spikes periodically throughout the simulation period (1000 ms for most tests). Each node has a distinct axonal delay $\mu = cd + \delta$, where cd is called *central delay* and is $\delta = nd \times \alpha$. The nd parameter is called *noise delay*, $\alpha = [(2x) - 1]$, and *x* is a uniformly distributed random variable in $[o, 1]$ that implements the axonal heterogeneity. Therefore, we analyze the signal propagation in the network to the chosen n_o. To collect more interesting data, we chose two input-output neurons with the largest distance between them in the structure. Only the initiator neuron spikes at the beginning of the simulation, after which the spike activity propagates to distant test neuron n_o. The simulation calculates the time it takes for the first spike to reach the chosen output node. We ran several simulations, increasing the noise delay using the randomly uniform distribution of α parameter x. Since the dis-homogeneity is random and uniform, we should not expect any advantage due to the noise. Instead, we will prove that it favors faster spiking activity propagation and we will give a simple theoretical framework to understand why.

Chapter 1

Chapter 1: Methods

1.1 Network

1.1.1 Izhikevich neuron model

Python and the NEST library version 2.2 [31] were used to create and connect neurons that mimic spiking networks continuously. NEST library allows the implementation of specific functions on large sets of nodes whose connections have a configurable delay/weight as well as parameters and state variables [32]. The neuron model, which reproduces the spiking and bursting behavior of known types of cortical neurons, is based on the one presented by Izhikevich [29]. Among several models for studying spiking neural networks (SNN), the type proposed by Izhikevich offers highly plausible biological dynamics, fundamental to reproducing well the non-linear phenomena dynamics of the neural network. Without realistic neuronal dynamics, we will not be able to explain the faster spiking activity propagation caused by the increased spatial heterogeneity in the network. The choice of a spiking neural model is extremely important to efficiently structure the network task. De facto, one of the most used prototypes to describe neural functionality in the field of neuron science is the LIF (leaky integrate-fire) model, considered simple while implemented at low computational cost [33]. However, the Izhikevich one is widely recognized as one of the most powerful and accurate models able to simulate thousands of neurons in real-time while offering a solid accuracy to reproduce spike patterns [34]. The model offers highly plausible biological dynamics and reproduces a large variety of spiking models by manipulating a few parameters. We used a Runge-Kutta method to process the Izhikevich model differential equations and a pipeline/buffer procedure to describe the delay's behavior within the NEST network. A weighted sum considers presynaptic input, where the weights represent synaptic connection strength parameters. When a neuron is delayed by a specific amount of time, its signal will continue to travel down a memory register *pipe*. This is so long as the delay is expressed as several time steps. In other words, at each time step, the pre-synaptic membrane potential is inserted at the beginning of the pipe, whereas the last element is fed to the Izhikevich differential equation. Since the pipe is rolled one step forward at each time step, and because it is as long as the delay, this method implements the time delay between pre-synaptic and post-synaptic neurons in a seamless manner without interfering with the theoretical models of delays in this study. Furthermore, by setting a few parameters, the Izhikevich neuron model reproduces most spiking activities, offering solid accuracy to reproduce spike patterns [34]. The Izhikevich neuron model describes the time evolution of the membrane potential v using a two-dimensional system of ordinary differential equations with four parameters a, b, c, and d which characterize both the spiking and the bursting behavior of the neurons [29]:

$$\begin{cases} v' = 0.04v^2 + 5v + 140 - u + I \\ u' = a(bv - u) \end{cases}$$

after the spike, a reset process is given by:

$$if\ v \geq 30mV\ \rightarrow \begin{cases} v \leftarrow c \\ u \leftarrow u + d \end{cases} \tag{1.1.1}$$

where $v' = \frac{dv}{dt}$, and $u' = \frac{du}{dt}$.

The variables v and u and the parameters a, b, c and d are all dimensionless [29], t is the time. In the mathematical model, v represents the membrane potential, and u is a membrane recovery variable, providing the negative feedback to v. After each spike, according to (1.1.1) the membrane voltage and the recovery variable are reset down to the parameter c and to $u + d$ respectively. I is the variable representing the external current stimulus, while the adjustment $0.04v^2 + 5v + 140$ allows the membrane potential v and time t to be scaled respectively to mV and ms. The parameters a, b, c, and d, according to their values, enable the equation to depict various firing pattern models.

In particular: The parameters of the Izhikevich more described respectfully:

- *a*[0.02]: recovery variable. An increment of *a* results in a quicker recovery for *u*.
- *b*[0.20]: underlines the strength of u to the sub-threshold fluctuations of the membrane potential v. An increment of b is translated into a stronger interrelation between u and v, meaning possible sub-threshold oscillations and low-threshold spiking dynamics. *u* to the subthreshold fluctuations of the membrane potential *v*.
- *c*[-65 mV]: the after-spike reset value of the membrane potential *v*.
- *d*[6 mV]: the after-spike reset of the recovery variable *u*.

When the membrane potential reaches a threshold value (typically around 30 mV), the neuron produces an action potential or spike, and the membrane potential is reset to a reset value (typically -65 mV) while the recovery variable *u* is increased by a reset parameter (typically *u* += *d*). The Izhikevich neuron model is known for its ability to replicate a wide range of spiking patterns observed in real neurons, including regular spiking, bursting, and fast-spiking. By adjusting the parameters (*a, b, c, d*) of the model, various types of spiking behaviors can be simulated. Overall, the Izhikevich neuron model provides a computationally efficient approach to studying the dynamics of spiking neurons and has been widely used in computational neuroscience and neural network modeling.

1.1.2 Network structure

In our network, we employ bidirectional communication between neurons, which is a communication pattern commonly observed in complex neural networks that are responsible for memory and cognitive functions. In such networks, information flows in multiple directions, allowing for the exchange of data and signals between neurons in both forward and backward directions. This bidirectional flow of information enhances the network's ability to perform sophisticated computations and respond to a wide range of cognitive tasks [35]. As a result, a viable connection structure must be established for each node or neuron to ensure the proper functioning of the model. When designing the dynamic network, one possible approach is to consider the von Neumann neighborhood type within an n-dimensional lattice, where every node is connected to its $[2 \times n]$ neighboring nodes. The configuration depicted in Figure 1.2 represents a *2*-dimensional grid, where each neuron establishes connections with its adjacent nodes in the north, south, east, and west directions. In the context of machine learning, the distance between nodes is quantified using the Manhattan distance, also known as taxicab geometry. Unlike the Euclidean distance, the Manhattan distance may yield multiple distinct paths with the same distance between two points, as illustrated in Figure 1.1.

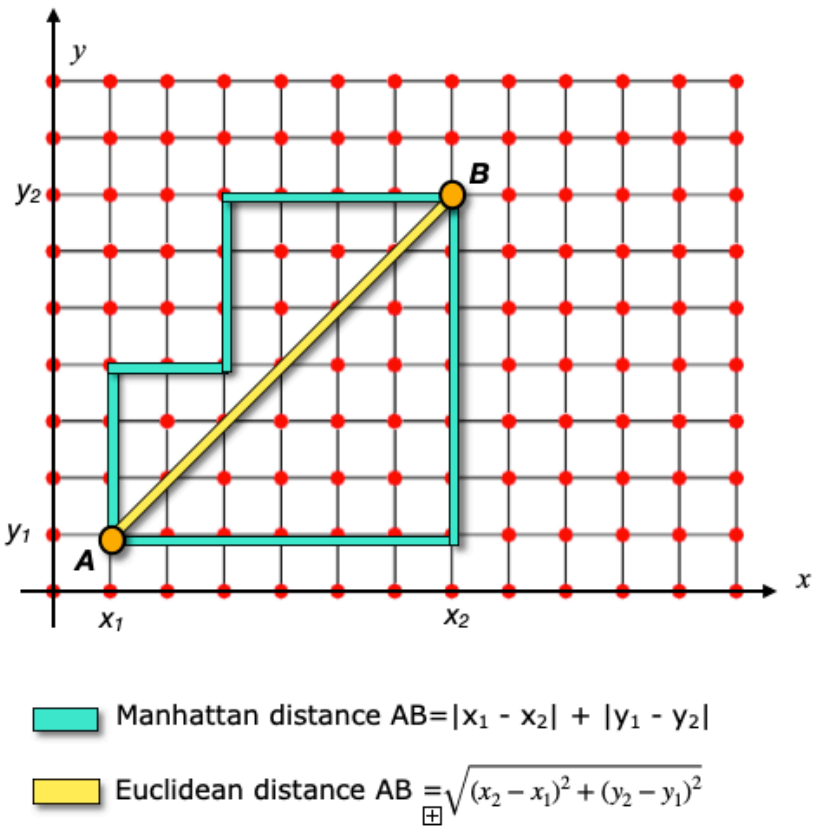

Figure 1.1: There are several shortest paths to go from *A* to *B*, but the Manhattan distance, which in this case is 12, is the same for any shortest path. Instead, in the case of Euclidean distance, there exists one and only one shortest path from *A* to *B*

We generate, therefore, a matrix grid of neurons connected according to the von Neumann neighborhood model. In the two-dimensional case, the first row is up-connected with the last row (and vice-versa), and the first column is left-arrow associated with the last column and vice-versa, as

in figure 1.2. The edges of the two-dimensional matrix grid are theoretically bent into a three-dimensional torus where a network representing a neural aggregate is arranged. This leads to similarities in toroidal neural networks (TNN) [36]. The toroidal structure opens the study of several appealing geometric interpretations.

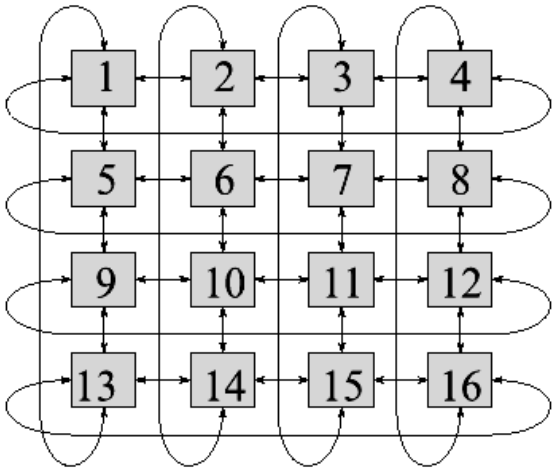

Figure 1.2: Toroidal network of 16 neurons plotted in 4×4 square matrices. To create a biologically plausible continuous system, that is to avoid the presence of boundaries or borders in the structure, the first row is connected to the last row and the first column to the last one.

For example, in Figure 1.3, the evolution of spike rates on a toroidal surface tends to approach a geodesic line, which is a local length-minimizing curve. From a topological perspective, the torus exhibits significant homeomorphic properties, which pave the way for further exploration in computational topology to enhance our comprehension of brain function (Coli, Tozzi).

After framing the network within a toroidal model and defining neurons according to the Izhikevich archetype, we conducted simulations. In the initial phase of the program, we constructed a matrix where nodes represent neurons interconnected in a pattern to form a toroidal grid consisting of 400 neurons (20×20 arrays). To maintain simplicity, all neurons are considered identical, devoid of inhibitory synapses and thalamic currents. Our primary focus lies in examining the impact of non-uniform axonal propagation delay (Madadi), so we investigate the model under pristine conditions. Specifically, we focus on regular spiking (RS) neurons, as they typify the most common neuron class in the cortex. To characterize the delay and connection strength for each neuron, we employ the following terminology. Each neuron is defined by its constant synaptic strength connection denoted as w, which remains consistent across the network and is not included in our calculations. The intrinsic axonal delay for each neuron is generally described by the variables $\mu = cd + \delta$, where cd represents the central delay, signifying the time taken for a spike to propagate along the axon, and δ represents random variation around this value (noise). Two main loops are involved in the process. The external loop iterates through the integer j, which controls the neuron's central delay (cd), while the internal loop iterates through i, which modulates the stochastic noise delay component (δ). We initially assign values to the variables *ns* (representing noise steps) and $(cd)_{max}$, which respectively denote the number

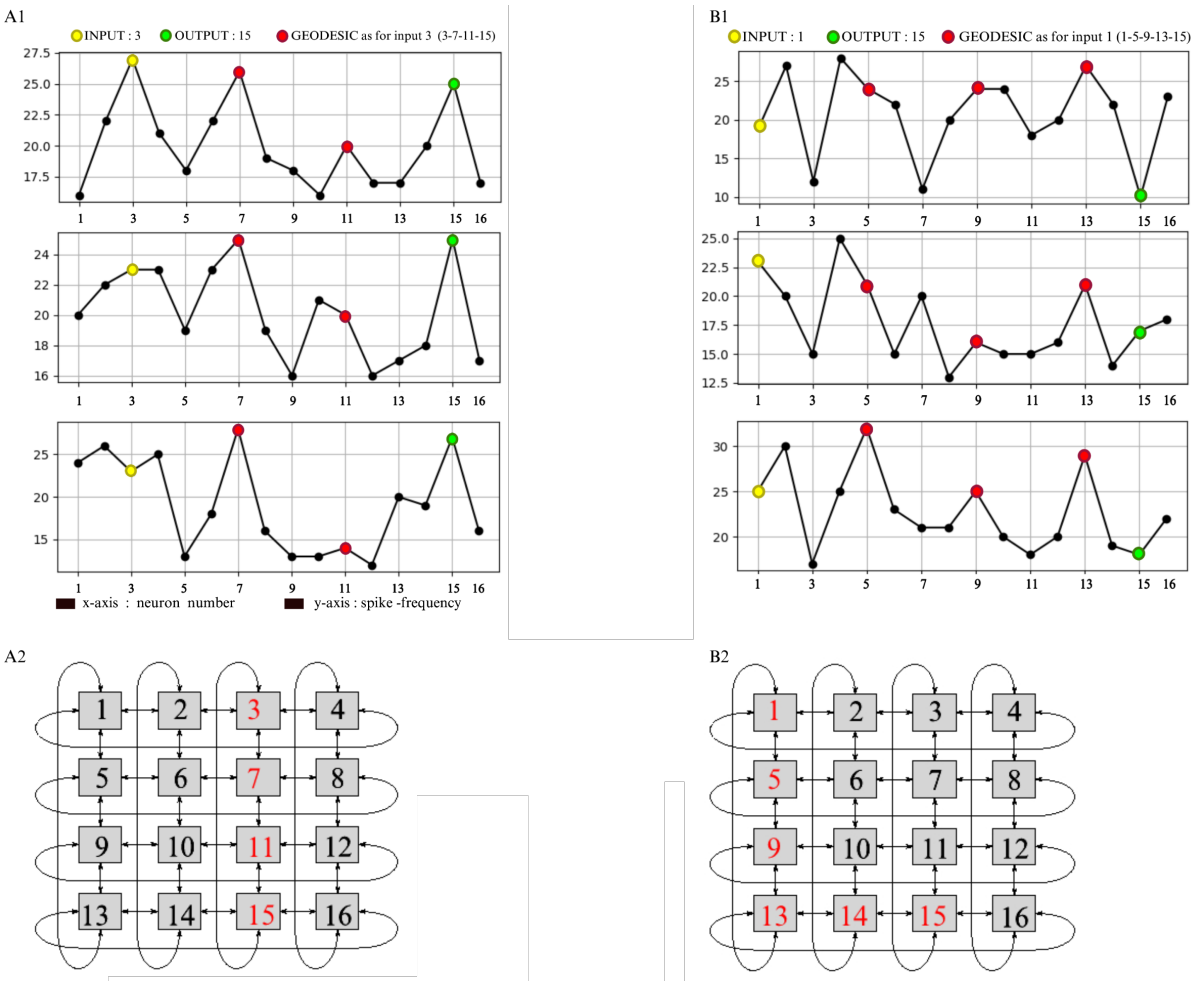

Figure 1.3: In *A1* and *B1* we run three simulations on the toroidal network of figure 1.2. Neuron 3 is considered the input of the network, being the only one connected to the external input and to initially spike. The three plots in *A1* show the spike rate calculated in three different simulations of 1000 ms. In *B1* other three simulations are shown, but this time the input neuron is in position 1. On *B1* the path 1-5-9-13-14-15 shows higher spiking frequency on the nodes 1-5-9-13, compared to paths with the same Manhattan distance as, for instance, the sequences 1-2-3-7-11-15 or 1-2-6-10-11-15. In *A1*, if we don't consider the direct connection 3 to 15, the shortest path from input(3) to output(15) is 3 steps. Nevertheless, a high spike frequency tends to lay on the path 3-7-11-15. Alternative paths with the same Manhattan distance are 3-2-14-15 and 3-4-16-15. In the three-dimensional torus, if we consider the Euclidean distance, the sequences in red in *A2* and *B2* (1-5-9-13) tend to lay on the longitudinal geodesic.

of iterations in the internal *i-loop* and the external *j-loop* as follows:

$$1 \leq i \leq ns \ , \ and \ \ 1 \leq j \leq (cd)_{max} \ , \ i, \ j \in \mathbb{N}$$

When *i* reaches *ns*, the central delay (*cd*) increases by 1. For simplicity, we consider $j = (cd)_j$ to assume the integers values (1, 2, 3, 4... $(cd)_{max}$). We indicate with $\mu^{i,j}_{n,n_k}$, the axonal transmission delay for a spike to travel between two neurons n, n_k. It is calculated at each simulation by a fixed delay equivalent for each neuron, referred to as *central delay* (cd_j), and its stochastic contribution $\delta^{i,j}_{f,f_p}$ as follows:

$$\mu^{i,j}_{f,f_p} = (cd)^j + \overbrace{i\frac{(cd)^j}{ns} \times \alpha^{i,j}_{f,f_p}}^{\delta^{i,j}_{f,f_p}} \tag{1.1.2}$$

where

* $\alpha^{i,j}_{f,f_p} = [2x^{i,j}_{f,f_p} - 1]$
* $(cd)^j =$ central delay; $1 \leq (cd)^j \leq (cd)_{max} \ , \ j \in \mathbb{N}$
* $\delta^{i,j}_{f,f_p} = i\frac{(cd)^j}{ns} \times \alpha^{i,j}_{f,f_p}$ such that: $-(cd)^j \leq \delta^{i,j}_{f,f_p} \leq (cd)^j$

  where $0 \leq x^{i,j}_{f,f_p} \leq 1$ is an aleatory variable with uniform distribution in $[0, 1]$ assigned to the connection of neuron n_f to n_{f_p} for each *i-loop* and *j-loop*, such that $-1 \leq \alpha^{i,j}_{f,f_p} \leq 1$.

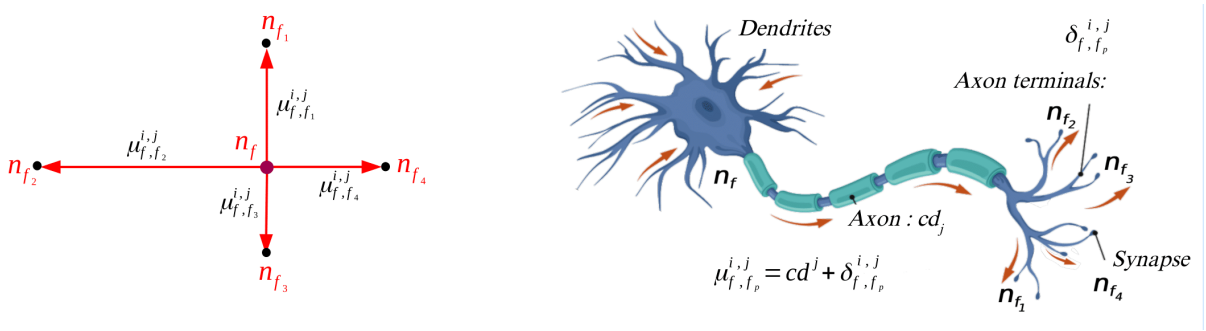

Figure 1.4: Biological representation of neuron

In Figure 1.4, on the right side, the biological representation of a neuron and its axonal delay transmissions are denoted as μ. The central delay, labeled as *cd*, simulates the neuron's axon, while δ simulates the axon terminal. The total distance comprising these two segments varies for each connection between n_f and n_{f_p}, as shown on the left side of the figure. The simulation starts with *j*=1 (*cd*=1). At each *i-loop*, each couple of neurons is assigned with an intrinsic delay $\mu^{i,j}_{f,f_p}$ where, respectively, j represents the *cd* (same for each couple of neurons), and i the increment of axonal heterogeneity. This framework realizes a network of neurons having a different (heterogeneous) intrinsic axonal transmission delay $\mu^{i,j}_{n,n_k}$. In the whole network, only n_{in} is stimulated by an external current $I = 10$mA, as suggested by Izhikevich [29]. Once this spikes regularly, its activity propagates to its neighbors with a certain delay, and so on. Hence, we measure the propagation of spike activity between two defined neurons. The initiator n_{in} and random neuron n_o. The subscripts in and o stand loosely for *initiator* and *output* respectively.

Consequently, we define:

- $f_{out}^{i,j}$ as the time of the first spike of n_o.
- $f_{in}^{i,j}$ as the time of the first spike of n_{in}.

And, accordingly the *spike propagation delay* from n_{in} to n_o as:

$$\Delta f_g^{i,j} = f_{out}^{i,j} - f_{in}^{i,j} \tag{1.1.3}$$

In the context where *g* represents the minimum Manhattan distance (*mMd*) from n_{in} to n_o, among the two neurons [37] [36], a specific $\Delta f_g^{i,j}$ is given for each i. For every complete iteration of the *i-loop*, a collection of *ns* values is assembled. All $\Delta f_g^{i,j}$ within one *i-loop* share the identical central delay $(cd)^j$. As *i* progresses to *ns*, the central delay $(cd)^j$ is increased by 1, initiating a new cycle of *i-loop*s. Upon *j* reaching $(cd)_{max}$, the simulation concludes. The primary aim is to assess whether the increment of axonal heterogeneity impacts spike signal transmission. Specifically, the focus is on determining if as *i* increases it corresponds to a reduction in $\Delta f_g^{i,j}$. To achieve this, we calculate the regression line of the $\Delta f_g^{i,j}$ for each *i-loop*.

1.1.3 *SGE*: Stochastic Grid Enhancement

To elucidate the impact of axonal heterogeneity on spike propagation, our initial analysis involves tracking the temporal evolution of spike activity propagation within the network while maintaining a constant delay value. In Figure 1.5, we set the delay parameter to (cd) = 50 milliseconds and calculate $\delta = (cd)/4 = 12$ milliseconds. We monitor the 'time of the first spike' for all neurons in the network, with only neuron n_{in} exhibiting initial spiking activity. The propagation of the spiking signal commences from neuron n_{in} and propagates through the network. As anticipated, we observe a linear relationship between the Manhattan distance from the test neuron and the initiator neuron. In our specific scenario, the network comprises a grid of 20 × 20 neurons. We identify each neuron with an index based on its position within the grid. By placing the initiator in the center of the second row, it is assigned an index of 30 (20 neurons in the first row and an additional 10 neurons for the central position in the second row). Following this indexing convention, we investigate the time of arrival of the spike-wave for each neuron along the geodesic path toward the output neuron 230, which is also positioned on the geodesic line in the central row. As evident from the simulation results depicted in Figure 1.5, the propagation delay in milliseconds exhibits a linear increase with distance, aligning with our intuitive expectations.

We now proceed to assess whether the introduction of axonal heterogeneity has a positive impact on the propagation of spiking activity throughout the neural network. In Figure 1.6, we present two maps depicting the toroidal network under varying noise levels. Each pixel within these maps corresponds to an individual neuron, with its color indicating the time of the first spike in milliseconds. Notably, neuron n_{in} is situated at coordinates x=10, y=2 on the grid, indexed as 30. The remaining neurons exhibit spiking activity that follows the axonal propagation delay

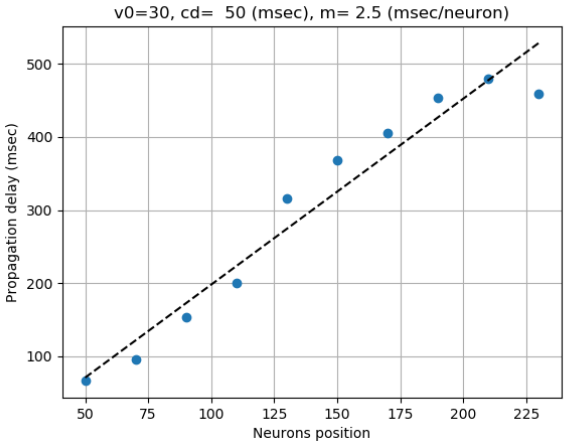

Figure 1.5: The spike activity propagation delay on the torus. Here the first spike happens at time $t = 0$ at the node located at index 30, the delay is calculated when the neuron at the node in the position indicated on the horizontal axis has its first spike. The tested neurons are those located at the geodesic of the toroidal grid. In these tests, the intrinsic delay and delay heterogeneity are kept constant at $cd = 50$ ms and $\delta = 12.5$ ms respectively.

across the network. When we reduce the level of axonal heterogeneity, as illustrated in Figure 1.6 (A), we observe a corresponding decrease in the number of neurons reached by the spiking activity, represented by deep purple regions on the map. Conversely, an increase in axonal heterogeneity level, as depicted in Figure 1.6 (B), results in an expansion of the area covered by spiking activity. Our findings indicate that elevating the degree of axonal heterogeneity leads to a reduction in propagation delay. Furthermore, in the context of Equation (1.1.3), as the axonal heterogeneity parameter ($i \to ns$) is heightened, the value of $\Delta {f_g}^{i,j}$ tends to decrease.

To describe the effect of axonal heterogeneity from an analytical point of view, we reckon the general equation for the regression line [38]:

$$\bar{y} = \widehat{m}\bar{x} + \widehat{\alpha}$$

where

$$\widehat{m} = \frac{\sum_{i=1}^{n}(x_i - \bar{x})(y_i - \bar{y})}{\sum_{i=1}^{n}(x_i - \bar{x})^2} = \frac{\sigma_{x,y}}{\sigma_x^2} \tag{1.1.4}$$

Here we introduce

$\bar{x}$ and $\bar{y}$ as the average of the x_i and y_i.

σ_x and σ_y as the standard deviations of$x$ and y.

σ_x^2 and $\sigma_{x,y}$ as the variance and covariance.

We pose $i\frac{(cd)^j}{ns} = (nd)_{i,j}$; such that in our model $(x_{i,j}; y_{i,j}) = ((nd)_{i,j}; \Delta f^{i,j})$.

We now try to give a mathematical formulation for m and prove that since from our data $m < 0$, then we must have, in general, $\Delta f^{(i,j)} < \Delta f^{(e;j)}$ when $e \leq i$. In other words, when the noise $\delta_{i,j}$ increases, the delay $\Delta {f_g}^{i,j}$ decreases. From (1.1.4) we calculate the slope for the linear

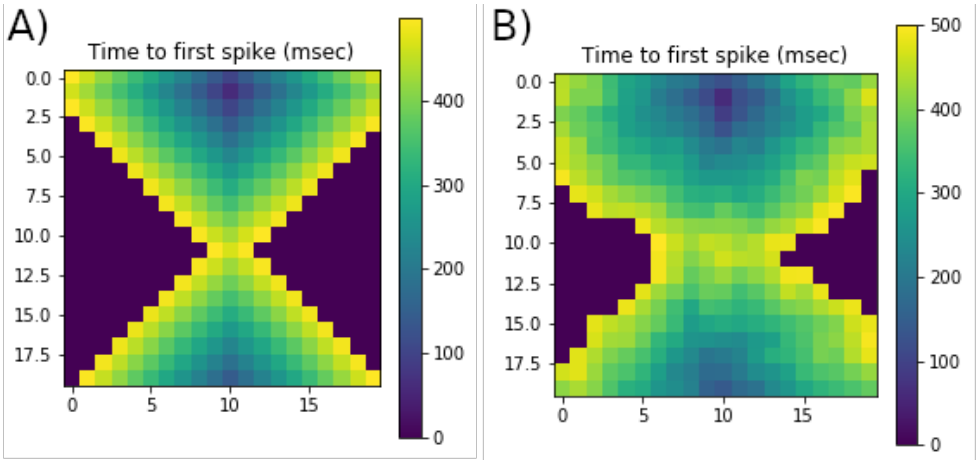

Figure 1.6: In this analysis, we present the temporal delay of spikes for each neuron within a 20x20 toroidal network. Specifically, we provide the timestamp at which the first spike occurs for every neuron in the network, signifying the moment when each neuron first receives spiking information. The neuron n_{in} located at index 30 with coordinates x=10 and y=2 on the map, commences spiking at t=0 in response to a constant input current of I0=10 mA. The color bar is utilized to represent the timing of the first spike for each neuron in milliseconds. The areas depicted in dark blue on the map signify regions where neurons fail to spike within the given time frame of our test simulation, which spans 500 ms. This occurs when the spiking activity initiated by the 'initiator' neuron n_{in} does not propagate to these regions promptly. Notably, in the first panel, where the noise level is minimal, a significant portion of the network remains untouched by the spiking activity. In contrast, in the second panel, where the noise level is higher, the circulation of spikes is accelerated, resulting in a greater number of neurons being influenced by the n_{in}'s activity.

regression [1], where:

$$\sigma_x^2 = \frac{\sum_{i=1}^{ns}(x_i - \bar{x})(x_i - \bar{x})}{ns} \tag{1.1.5}$$

$$\sigma_{x,y} = \frac{\sum_{i=1}^{ns}(x_i - \bar{x})(y_i - \bar{y})}{ns} \tag{1.1.6}$$

our respective values are:

- $x_i^j = (nd)_{i,j} = i\frac{(cd)_j}{ns}$; $\bar{x} = \frac{(cd)_j(ns+1)}{2ns}$
- $y_i^j = \Delta f^{i,j}$; $\bar{y} = \frac{\sum_{i=1}^{ns}\Delta f^{i,j}}{ns}$

To simplify the symbolism from now on we reckon $cd_j = cd$, and $\Delta f^{i,\,j} = \Delta f^i$. We omit the index *j* since cd_j is constant during the calculation of a single *m* while only *i* ranges from 1 to *ns*. By substituting $x_i,\ \bar{x},\ y_i,\ \bar{y}$ respectfully in (1.1.5) and (1.1.6), we get:

$$\sigma_x^2 = \frac{\sum_{i=1}^{ns}(x_i - \bar{x})^2}{ns} = \frac{(cd)^2}{ns^2}\frac{(ns^2-1)}{12}$$

and

$$\sigma_{x,y} = \frac{(cd)}{ns^2}[\sum_{i=1}^{ns}(i\Delta f^i) - \frac{(ns+1)}{2}\sum_{i=1}^{ns}\Delta f^i]$$

[1] It is just reported a part of the demonstration.

which we can write as:

$$\sigma_{x,y} = (cd)ns^2 \sum_{i=1}^{\frac{ns-1}{2}} |(i - \frac{ns+1}{2})|(\Delta f^{(ns+1-i)} - \Delta f^i)$$

From (1.1.4) we can formulate:

$$m = \frac{\sum_{i=1}^{\frac{ns-1}{2}} |(i - \frac{(ns+1)}{2})|(\Delta f^{(ns+1-i)} - \Delta f^i)}{(cd) \cdot \frac{(ns^2-1)}{12}}$$

We have $m < 0$ only if the numerator is negative, therefore, for most of the Δf^i, it must follow:

$$\Delta f^{(ns+1-i)} < \Delta f^i \tag{1.1.7}$$

.

The (1.1.7) demonstrated how, by increasing the index *i* (i.e., noise), the delay of a signal is reduced compared to the preceding one. As a result, we can conclude that increasing noise reduces the delay of a signal from input to output for a fixed central delay $(cd)_j$.

We varied the intrinsic axonal delay parameter $(cd)j$ across a range of values, spanning from 1 to 100 milliseconds. For each of these values, we conducted experiments involving forty different noise levels, ranging from $(cd)j/40$ to the maximum delay value $(cd)max = 100ms$. The top panels of figures 1.7 and 1.8 illustrate the distribution of spike arrival times in the *output* neuron n_o. In figure 1.7, with a relatively large central intrinsic delay of 93 ms, only 20 arrival times are observed. Our simulation has a duration of 1000 ms, and depending on the stochastic $\delta i, j$ factor's variability, in certain cases, neuron n_o does not spike, as the information from neuron n_{in} doesn't arrive in time. Conversely, in figure 1.8, when the central delay is around 31 ms, the histogram is complete, displaying 40 arrival times concentrated at a shorter delay of approximately 350 ms. The central panels of these figures depict the first spike time in n_o for increasing values of $(nd)_{i,j}$. The linear regression's dark dotted line illustrates the significant trend of time decreasing as noise levels increase. Notably, when examining the bottom panels of both figures, the regression slope *m* consistently remains negative, and the minimum value occurs around *cd* = 35 ms (with the y-axis reversed). The bottom panel of figure 1.7 presents the values of *m* for each *cd*, spanning from the first to the last simulation (i.e., $2 \leq cd \leq 93.07$). We were able to replicate the minimum *m* value around *cd* = 35 ms in repeated simulations with different random seeds. The maximum value of *m* consistently occurred within a global minimum range of $30 \leq cd \leq 35$.

The consistent negativity of the slope *m*, which signifies how axonal heterogeneity diminishes the propagation speed within the network, persists across all conducted simulations. The replicable nature of this behavior underscores the robustness of this feature in our model neural network

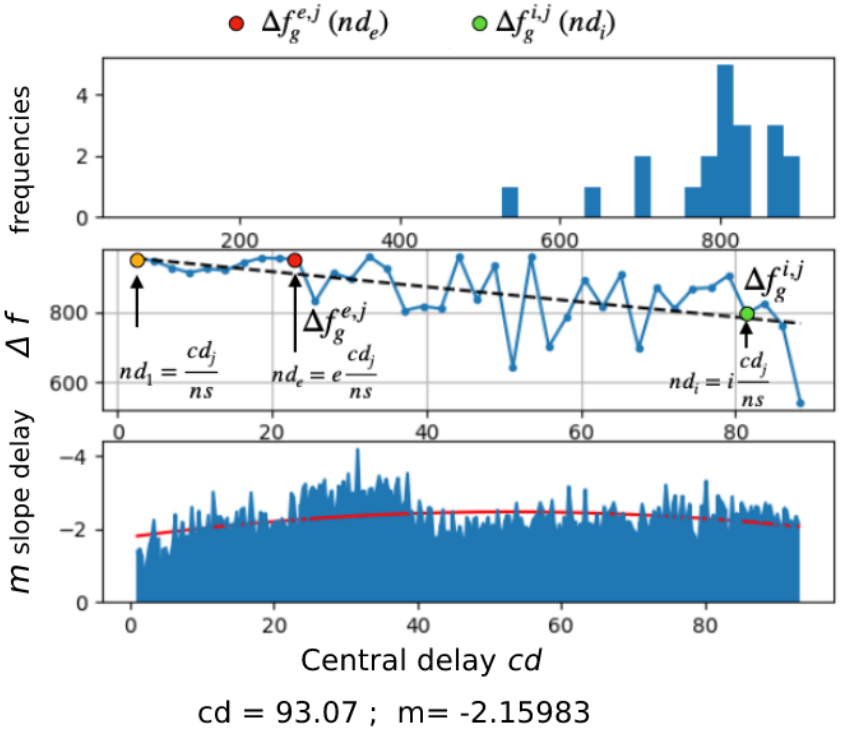

Figure 1.7: In the top panel, we plot the histogram of the time difference between the first spike of the *output* neuron n_o and the first spike of the *initiator* n_{in}. These times represent the times of arrival of spiking activity from an *initiator* neuron placed at position 30 to a *test* or *output* neuron placed far away in the toroidal network (in position 230). We performed 40 simulations with increased noise levels, from $cd/40$ ms up to $cd = 100$ milliseconds. The resulting histogram is centered around a delay difference $\Delta f_g^{i,j}$ of about 800 milliseconds. In the central panel, we plot the same arrival time differences in the function of the noise $(nd)_{i,j}$. We have 40 increasing values of $(nd)_{i,j}$ from 1 to $(cd)_j$ (cd is fixed in these plots to $(cd)_j = 93.07$). We notice that for a small value of heterogeneity ($(nd)_{i,j}$ between 0 and 23), the delay difference doesn't change much, settling on values greater than 800. Eventually, by increasing the noise, $\Delta f_g^{i,j}$ decreases accordingly, reaching values below 800 ms. The dotted line represents linear interpolation with an inclination of $m = -2.15$, as indicated in the figure's title. In the bottom panel, we plot all the values of m obtained by previous simulations, where each has a different neuronal intrinsic delay $(cd)_j$ (ranging from 5 to 100 ms in 1 ms steps). While the top and central panels refer only to the value of $(cd)_j = 93.07$, the bottom panel reports all the previous values of m up to the current $(cd)_j$. A negative m indicates that the delay value is decreasing.

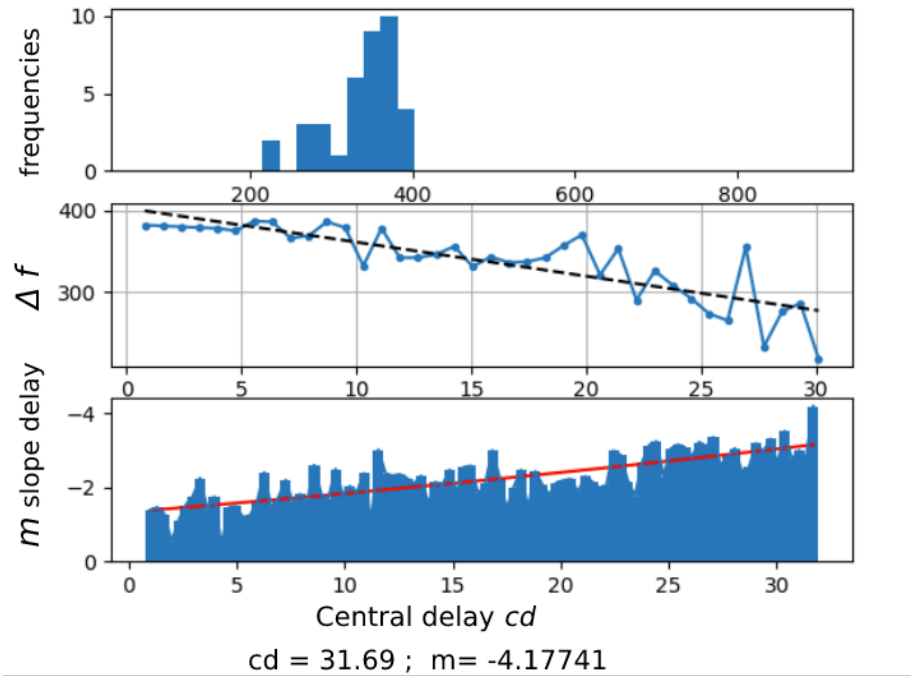

Figure 1.8: Same as figure 1.7. Precisely, we present the value of *m* corresponding to the global minimum for *m*=-4.17 (in the graph, minimum appears as a maximum as the ordinate are inverted for clarity). The biggest effect of delay difference was observed in all of our testings for intrinsic delay values in the range $31 \leq cd \leq 35$. When the intrinsic delay is centered at 35 ms, the signal from n_{in} propagates faster.

1.1.4 Process time

The following section offers a theoretical interpretation of the negative aspects associated with the variable denoted as m. Our investigation delves into the dynamic characteristics of neurons, necessitating a comprehensive comprehension of the phase portrait of the membrane potential and recovery system. The phase space features various conditions, including equilibrium, limit cycles, attractors (as described by Izhikevich [29]), and other properties that aid in elucidating the spiking behavior from a dynamic systems perspective. In this analysis, we examine two distinct phases, commencing with the scenario in which a neuron resides in an equilibrium state, characterized by a resting membrane potential [39]. In Figure 1.9.1 of the phase space plot shown in Figure 1.9.2, input currents induce a minimal presynaptic potential (PSP) [40]. In this phase diagram, the membrane potential exhibits slight deviations from the equilibrium point (represented as a black spot or an attractor corresponding to the resting potential). Subsequently, after a few milliseconds, it returns to its resting state.

Instead, in figure 1.9 panel 3, we show the effect of two pre-synaptic stimuli. A little signal PSP (A) causes a slight change in the equilibrium, whereas a bigger signal PSP (B) causes the neuron's intrinsic dynamics to spike after a short time. The period between the arrival of the stimulus and the realization of the spike is referred to as *process time*. Now we'll look at what happens when a PSP signal A reaches a post-synaptic neuron while that same neuron is still firing as a result of a prior PSP signal B. Consider the case where a spike leaves a neuron n_f and travels in the direction of neuron n_{f1}.

Firstly we define:

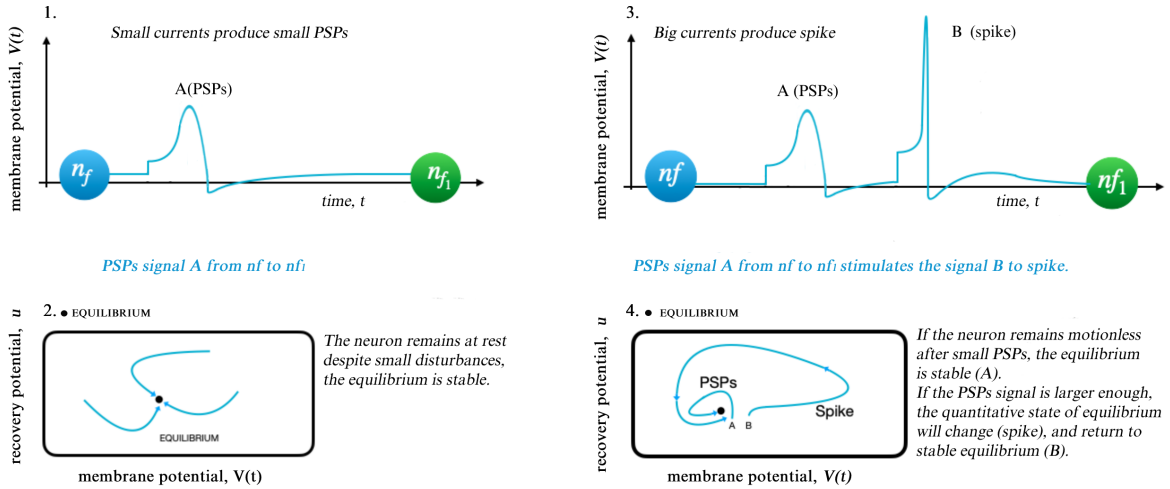

Figure 1.9: *Panels 1 and 2: a stable equilibrium. A small pre-synaptic signal (PSP) goes from neuron n_f to n_{f_1}. The membrane potential will fluctuate around the equilibrium point before returning to its resting state (black dot, the equilibrium point). Panels 3 and 4 depict the responses of two different pre-synaptic stimuli. The small PSP (A) doesn't induce a spike, whereas a bigger PSP (B) does. The time it takes for the neuron to achieve a spike following the PSP is referred to as process time, and it is measured in milliseconds as in the Izhikevich regular spiking neurons employed in our model.*

- Process time $\tau_{f_p}^{i,j}$: that represents the time for neuron n_f to *process* a pre-synaptic spike and deliver its post-synaptic spike, the two indexes i and j represent the current central delay $(cd)^j$ and its stochastic variation $\delta^{\,i,j}$.
- Axonal transmission delay $\mu_{f,f_p}^{i,j}$: the time for a spike to go from neuron n_f to one of its four adjacent neuron $n_{fp,(p=1,2,3,4)}$, as in eq.(1.1.2).
- Total transmission Delay $d_{f,f_p}^{i,j}$:

$$d_{f,f_p}^{i,j} = \mu_{f,f_p}^{i,j} + \tau_{f_p}^{i,j} \tag{1.1.8}$$

The random variable $x_{f,f_p}^{i,j}$, characterizes the delay transmission from n_f to n_{fp}, and a process time $\tau_{f_p}^{i,j}$. Therefore, each *i-simulation* defines $d_{f,f_p}^{i,j}$. Once everything is in place, the network operates as expected: a spike reaches a specific input neuron n_f. The neuron n_f will process the signal with a processing time τ_{f_p}. Subsequently, the spike leaves n_f and reaches four adjacent neurons $n_{fp,(p=1,2,3,4)}$ with four different axonal transmission delays $\mu_{f,\,f_p}^{i,\,j}$ defined in equation(1.1.2). We now want to focus on the case when :

$$\mu_{f,f_p}^{i,j} < \tau_{f_p}^{i,j} \tag{1.1.9}$$

Following equation (1.1.9), the spike generated by neuron n_f is anticipated to reach neuron n_{f_1} promptly, even as the post-synaptic neuron is still in the process of handling the signal from B'. The amalgamation of these two membrane potentials, as illustrated in the phase diagram depicted in Figure 1.9.4, serves to expedite the generation of a spike, thereby reducing the processing duration denoted as $\tau_{f_p}^{i,j}$. Consequently, the overall time interval spanning from the

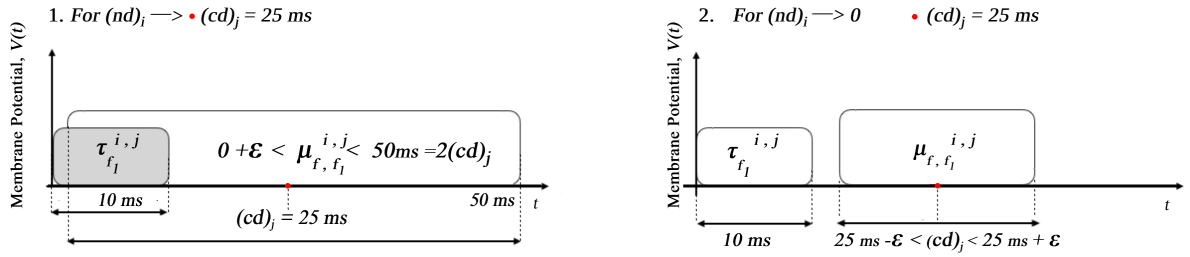

Figure 1.10: A sketch representing how the variability of the axonal delay influences the overall spike activity propagation along with the network. Two cases are shown: in panel 1. the variability of the axonal transmission $\mu^{i,j}_{f,f_p}$ is wide (from zero to 50ms in this example where the central value of the delay is 25ms). Since this value can become smaller than the processing time $\tau^{i,j}_{f_p}$, this will positively influence the phase space of the neuron's dynamic, resulting in a faster post-synaptic response. In panel 2 it is shown the opposite situation in which the variability of the axonal delay is smaller and never realizes this condition. Since a longer than average, $\mu^{i,j}_{f,f_p}$ doesn't increase post-synaptic process times, whereas a shorter than average does, this indicates how a degree of randomness helps the overall circulation of spike activity on the toroidal network.

initial pre-synaptic stimulation initiated by A′ to the eventual post-synaptic spike, labeled as $d^{i,j}_{f,f_1}$, undergoes a reduction. In simpler terms, owing to the stochastic variability inherent in axonal transmission delays denoted by $\mu^{i,j}_{f,fp}$, the temporal delay may fluctuate randomly, either exceeding or falling short of the mean value. In instances of shorter delays, the arrival of a second spike at the post-synaptic neuron leads to decreased processing times. Conversely, when $\mu^{i,j}_{f,fp}$ is higher, the processing times $\tau^{i,j}_{f_p}$ remain unaffected. This inherent asymmetry in the system accounts for the observed phenomenon in our simulations. As the degree of axonal heterogeneity in the network increases, the likelihood of this condition occurring across multiple neurons rises, resulting in accelerated propagation of spiking activity and enhancing the overall flow of information throughout the network. For a visual representation of this phenomenon, please refer to Figure 1.10.

In Figure 1.11, we provide a schematic illustration of the operational principles of the *SGE effect* concerning the temporal aspects of processing time τ depicted in red, and transmission time μ represented by the blue line. Our theoretical framework postulates that the presence of processing time τ is a prerequisite for the occurrence of the *SGE effect*. In this context, transmission time μ, given a fixed central delay, signifies the duration required for an impulse to traverse the spatial gap between two neurons, whereas τ denotes the interval during which a neuron emits a post-synaptic spike after the arrival of pre-synaptic stimulation. The very existence of this mechanistic framework leads us to propose that during the τ interval, while a prior signal is undergoing processing, as denoted by (PSPs)B in the nf region of the plot, there exists the potential for another spike to propagate from the same source, *nf*, thereby expediting the emission process and ultimately facilitating the manifestation of the "SGE" effect.

1.1.5 *SNE*: Stochastic Neuron Enhancement

The initial type of heterogeneity manifests as non-uniform spatial gaps between neurons, achieved through the introduction of random axonal delays. This results in accelerated information trans-

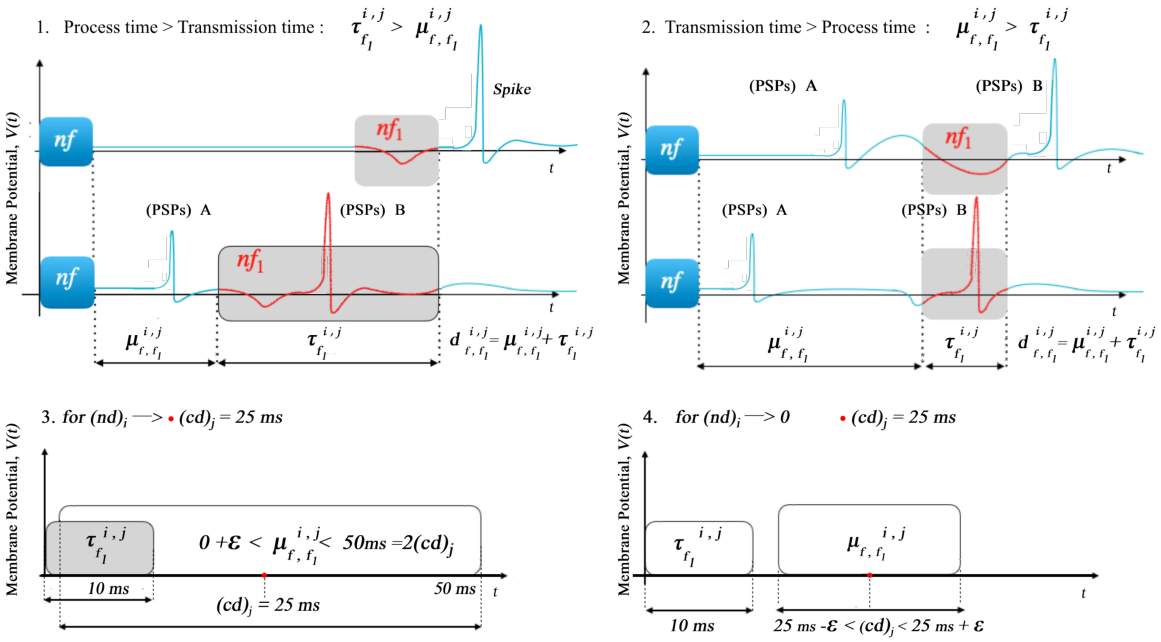

Figure 1.11: Representing how the variability of the axonal delay μ, triggers the *SGE* effect influencing the overall network's spiking activity. Two cases are shown: Process time $>$ Transmission time (panel 1.,3.) and Transmission time $>$ Process time (panel 2.,4.). In panel 3 we see how increasing the randomness results in a wider range of variability of $\mu^{i,j}_{f,fp}$ from 0ms to 50ms, with a central value of 25ms. In this case, μ can become smaller than the processing time $\tau^{i,j}_{fp}$, and positively influence the phase space of the neuron's dynamic, provoking a faster postsynaptic response. In panel 4, for a small randomness level, the variability of μ never gets below the value of τ and the *SGE* effect won't take action.

mission, denoted as *SGE effect*. The second type of heterogeneity revolves around a neural model that lacks uniformity. In this scenario, we manipulate neuron cell types by adjusting the parameters of the Izhikevich model, thereby altering various differential characteristics of the neurons and influencing their spike patterns and dynamics (see Figure 1.12). The simulations demonstrate that heterogeneity amplifies the overall number of spikes throughout the network, suggesting an augmentation in information robustness. Our findings align with recent notable studies, indicating that heterogeneity confers various advantages to the brain, including improved coding efficiency, enhanced reliability, superior working memory, and other functional attributes [20]. Henceforth, we shall refer to this phenomenon, stemming from the stochastic nature of the neuronal model, as "Stochastic Neuron Enhancement" (*SNE effect*).

1.2 Simulation on multidimensional networks

We will now explore the impact of the combination of *SGE-SNE* effect on various lattice grids, spanning dimensions two, three, and four, along with their associated toroidal frameworks. For instance, when considering a 3D lattice grid, we observe the emergence of a 4D toroidal network, where each neuron is surrounded by six adjacent neighbors, as opposed to four. To achieve the 4D torus, we achieve this by connecting opposite surfaces of the cube, creating a toroidal network that exists in a four-dimensional Clifford torus [41].

By employing a comparable idea, we can expand this to encompass a four-dimensional grid,

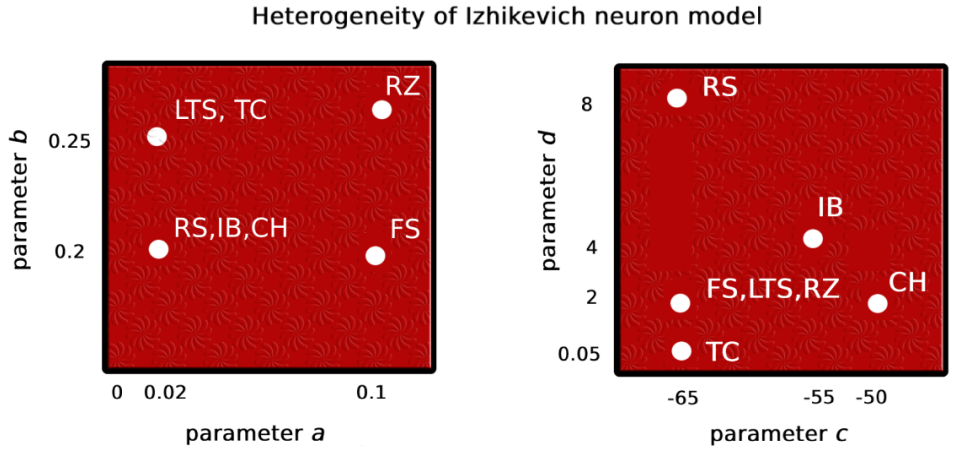

Figure 1.12: To different values of the parameters, *a, b, c, d*, correspond different types of Izhikevich neuron models as described by equations (1.1.1). In our simulation, the constant values of *a, b, c, d*=(0.02, 0.2, -65, 8) are congruent to a regular spiking (RS) model, while random changes of *c, d* correspond to a continuous variability of a large range of neuron models [29] such as IB (intrinsically bursting), CH (chattering), FS (fast-spiking), LTS (low-threshold spiking), TC (thalamocortical), RZ (resonator). The variability of *c, d* according to eq.(1.2.1), guarantees the neural heterogeneity of the model.

resulting in the formation of a torus situated within a five-dimensional space. In the following illustration, we present an overview of the connection between the dimensional grid and the corresponding toroidal network.

- 2D Lattice grid $\Longrightarrow$ Torus in 3D space
- 3D Lattice grid $\Longrightarrow$ Torus in 4D space
- 4D Lattice grid $\Longrightarrow$ Torus in 5D space

In the context of the three-dimensional topological arrangement [42], each node establishes connections with its six adjacent neighbors, enabling communication in six distinct directions: +x (east), -x (west), +y (forward), -y (back), +z (north), and -z (south). The four-dimensional torus structure naturally results in a von Neumann-shaped neighborhood [43], with cells being surrounded by six input connections [22]. In both scenarios, we introduce an external current of *I=10 mA* to an arbitrary neuron denoted as n_{in}, following the methodology presented in section (1.1). This current stimulates the neurons within the network, initiating the *SGE* effect. We subsequently examine the occurrence of this phenomenon on 2D, 3D, and 4D grids, investigate the impact of neural heterogeneity, and explore the influence of *SNE*. Finally, we consider the combined effects of both types of heterogeneities on the network.

In our model, we will keep *a, b* at constant values of 0.02 and 0.2, while the parameters *c, d* are heterogeneous, as in figure 1.12, will be subject to the form:

$$\begin{cases} c = -65 + (15 \times x_1 \times x_1) \\ d = 8 - (6 \times x_2 \times x_2) \end{cases} \tag{1.2.1}$$

$0 \leq x_1, x_2 \leq 1$: uniformly distributed random variables [29].

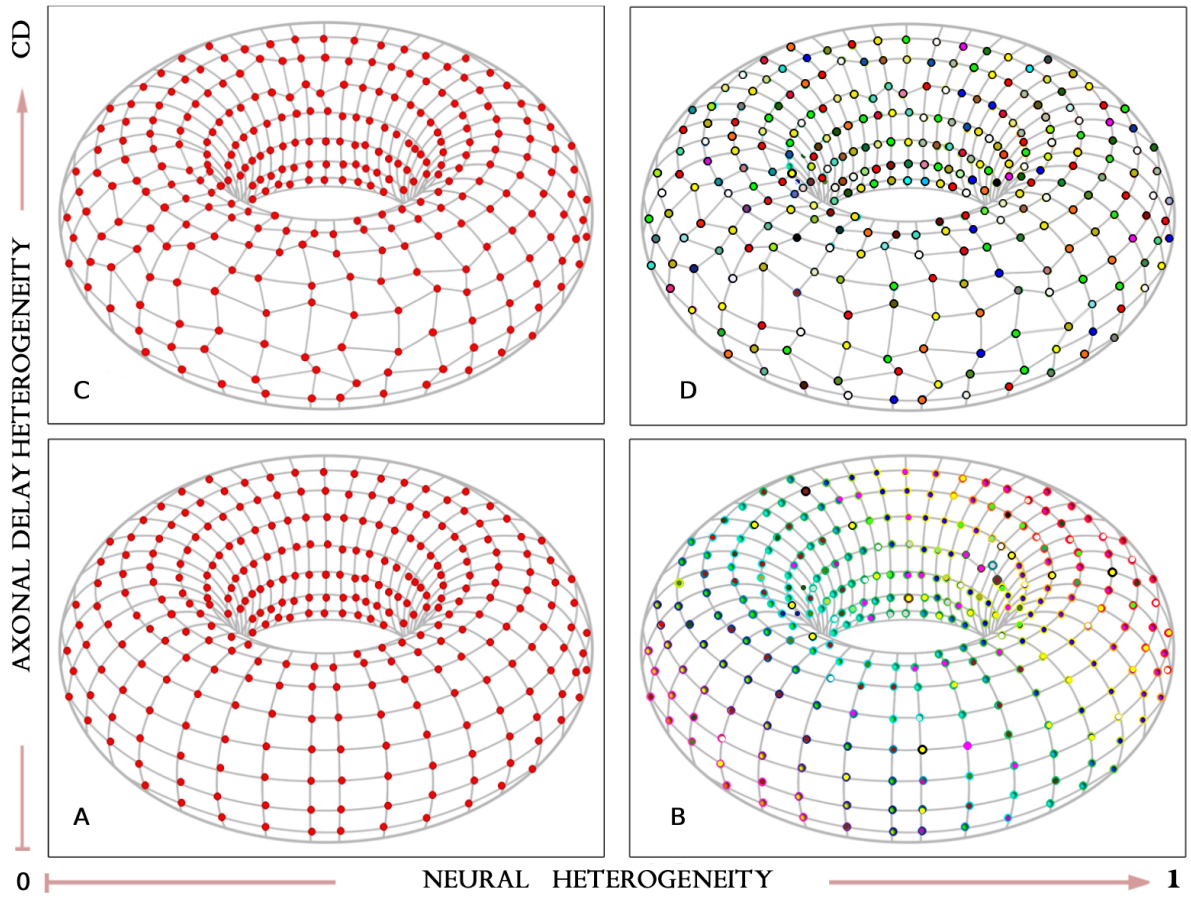

Figure 1.13: We present four distinct depictions of a 3D Torus derived from a 2D grid model. In this context, the network's neurons serve as nodes, and their edges are the axonal transmission delay $\mu_{f,f_p}^{i,j}$ defined in eq.(1.1.2). The *x-axis* signifies the extent of neural diversity denoted as H, which varies from 0 to 1. When H is at 0, all neurons are identical to each other, exhibiting neural homogeneity. Meanwhile, the *y-axis* illustrates the range of axonal heterogeneity, specifically the axonal delay δ^i, which spans from 0 to the central delay value *cd*. As δ^i varies, it results in differing values for the connections $\mu_{f,f_p}^{i,j}$.

A: In the specific scenario where H equals 0 and all δ^i are 0, the network grid exhibits regularity. As a result, all neurons are identical, denoted by the presence of red nodes, specifically of the R.S. Izhikevich type, and the axonal delay between them is uniform at the value of *cd* within a regular 3D layout.
B:Hypothesis H states that δ^i is equal to 0. Our approach focuses on altering neural heterogeneity exclusively by adjusting the parameters c and d in the Izhikevich neuron model. As depicted in Figure 1.12, this manipulation leads to the creation of a stochastic typology of neuron models. Importantly, the inter-neuron spacing remains fixed at the value of *cd*, while the varying colors of each neuron represent distinct Izhikevich neuron model types.
C: Under the conditions where H equals 0 and δ^i equals 1, all the neurons in the system are modeled as R.S. Izhikevich neurons. The variability in axonal delay between neurons is induced by axonal heterogeneity, as described by equation (1.1.2).
D: H: 1, and δ_i: 1. The illustration represents the utmost variability in structure, showcasing two forms of heterogeneity. It provides a visual representation of the most likely distribution of neuron populations in a network of diverse cells, where the inter-neuronal connection distances vary.

Heterogeneity of Izhikevich neuron model							
Parameters	RS	IB	CH	FS	LTS	TC	RZ
a :	0.02	0.02	0.02	0.1	0.02	0.02	0.1
b :	0.2	0.2	0.2	0.2	0.25	0.25	0.26
c :	-65	-55	-50	-65	-65	-65	-65
d :	8	4	2	2	2	0.05	2

Table 1.1: Values of the parameters *a, b, c, d* used for each model of figure 1.12.

In Figure 1.13 we show the effects of the combined heterogeneity on a 3D toroidal model network. Where the node's color variation represents the neural heterogeneity, the different distances of the connections illustrate the axonal delay heterogeneity.

We established three distinct networks in two, three, and four dimensions, each corresponding to a three-dimensional, four-dimensional, and five-dimensional torus, respectively. Subsequently, we conducted comparative simulations to scrutinize the outcomes. Initially, we constructed a three-dimensional matrix composed of 343 neurons, arranged in a $(7 \times 7 \times 7)$ grid, interconnected using the von Neumann neighborhood model, creating a toroidal structure by connecting opposing surfaces [36]. Once the network framework was established, we configured the neurons according to Izhikevich's model to initiate the simulations. Our primary focus in this study is to investigate the impact of non-uniform axonal propagation delay [44]. To begin, we examined the model in its simplest form, assuming that all regular spiking (RS) neurons were identical, without considering inhibitory synapses or thalamic currents. Subsequently, we will compare these results with those obtained from a model where neurons of the same size exhibit heterogeneity, and we will analyze the variations in the effects of heterogeneity.

1.2.1 Grid dimensions and *SGE* effect

We will now extend our analysis of the *SGE effect* phenomenon to various dimensions. We illustrate how this phenomenon becomes more pronounced when we increase the network's dimensionality. To begin, we explore the number of minimum paths with the same *mMd* between two random neurons in a lattice grid configured in a toroidal shape. The *mMd* from neuron n_{in} to neuron n_o represents the minimum number of steps required to reach n_o from $n_i n$, as depicted in Figure 1.14.

In a previous study involving a 2D lattice network (as described in [45]), each neuron had four adjacent neighbors. For any pair of neurons $[n_{in}; n_o]$, there were a specific number of paths with the same *mMd* that connected n_{in} to n_o. Given the network's structure, the most efficient way for a signal to reach the n_o was in *mMd* steps. In two dimensions, there were only two possible pre-synaptic connections to n_o, as shown in Figure 1.15(a). Initiating a path from one of the other two connections would require more steps than *mMd*. The strength of the *SGE* effect depends on the number of paths with the same *mMd*, which increases by manipulating the number of dimensions of the network and the nodes' coordinates as shown in the following.

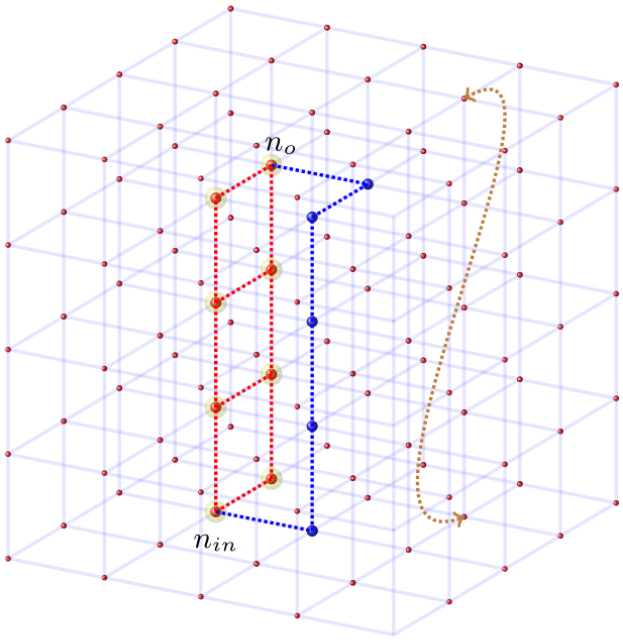

Figure 1.14: In this case, the *mMd* from n_{in} to n_o is 4. The red dotted lines represent all the possible paths with *mMd*, where all the others (as the blue dotted line) have a Manhattan distance $>$ *mMd*. In a 3D lattice grid, each node/neuron has six connections. The nodes on the border surface are connected with their respective counterparts on the opposite face. For clarity, the brown dotted line represents one of those cyclic connections. This structure is equivalent to a torus in 4D space.

Mathematical proof

Let's consider the following 3D cubic lattice (4D torus):

- side: $ln = 2 \times sl$
- coordinates of [(n_{in}, n_o)]: [(x_0, y_0, z_0); (x_1, y_1, z_1)]

We can formulate :

$$X = \begin{cases} |x_0 - x_1| & ; \text{if} : |x_0 - x_1| \leq sl \\ ln - |x_0 - x_1| & ; \text{if} : |x_0 - x_1| > sl \end{cases} \tag{1.2.2}$$

$$Y = \begin{cases} |y_0 - y_1| & ; \text{if} : |y_0 - y_1| \leq sl \\ ln - |y_0 - y_1| & ; \text{if} : |y_0 - y_1| > sl \end{cases} \tag{1.2.3}$$

$$Z = \begin{cases} |z_0 - z_1| & ; \text{if} : |z_0 - z_1| \leq sl \\ ln - |z_0 - z_1| & ; \text{if} : |z_0 - z_1| > sl \end{cases} \tag{1.2.4}$$

In this context, the variables *X, Y*, and *Z* represent the minimum number of steps required along each dimensional axis to go from n_{in} to n_o. This definition aligns with the concept of the minimum Manhattan distance, which can be expressed as *mMd* = *X* + *Y* + *Z*. For instance, suppose our calculations yield the values (*X, Y, Z*) = (3, 4, 5). Consequently, the minimum number of

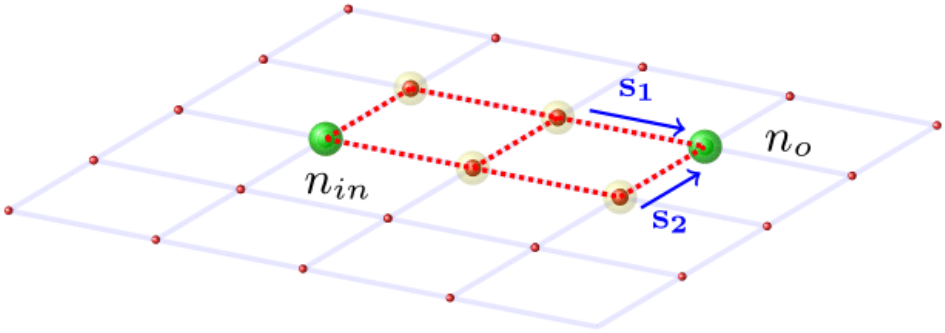

(a) mMd: 3 ; Number of paths: 3

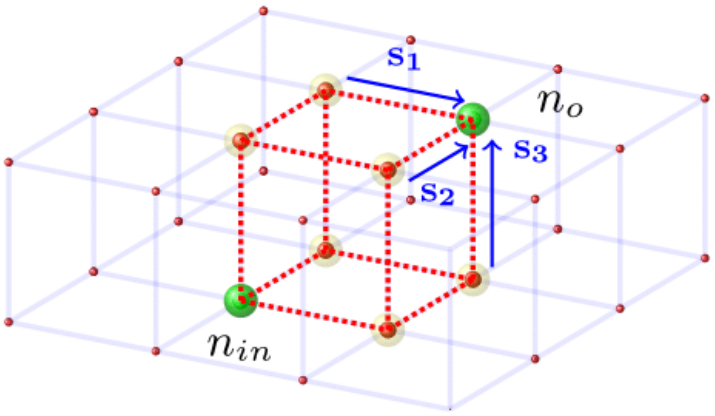

(b) mMd: 3 ; Number of paths: 6

Figure 1.15: Illustration of a network in both 2D and 3D is presented. When we contrast these two network representations, it becomes evident that as we elevate the dimension, the quantity of pathways with identical *mMd* also increases proportionally. Moreover, the presynaptic activity experiences an uptick in the higher-dimensional network, consequently amplifying the likelihood of observing the *SGE effect*.
In panel (a), within the two-dimensional grid, there exist three distinct routes from n_{in} to n_o, each with a *mMd* value of 3. Under these circumstances, there is a possibility of having up to two presynaptic signals, denoted as s_1 and s_2, arriving at n_o almost simultaneously, thus instigating the *SGE effect*.
In panel (b), the three-dimensional grid creates six distinct routes, all with an identical *mMd* value of 3, connecting n_{in} to n_o. In this scenario, the presence of a greater number of routes allows for the simultaneous convergence of up to three presynaptic signals, denoted as $s_1, ; s_2, ; s_3$, at n_o, thereby enhancing the likelihood of the *SGE effect* becoming significant.

steps to traverse from n_{in} to n_o is *mMd* = 3 + 4 + 5 = 12. To elaborate, one could start at n_{in}, take 3 steps along the *x-axis*, followed by 4 steps on the*y-axis*, 5 steps on the *z-axis*, and then conclude with 2 more steps on the *y-axis*. This path from n_{in} to n_o illustrates an *mMd* of 12.

Our objective is to determine the total number of paths with an *mMd* of 12. Intuitively, this can be achieved by permuting the partitions of *X, Y*, and *Z*, and the precise solution can be obtained using the multinomial coefficient [46]:

$$P = \frac{(X+Y+Z)!}{X!\,Y!\,Z!} \tag{1.2.5}$$

P represents here the number of paths with the same *mMd*=*X*+*Y*+*Z* from n_{in} to n_o in the 3D lattice grid. By keeping n_{in} in the same position, if we increase the number of dimensions of the grid, we may expect the number of paths with the same *mMd* to increase accordingly (as in figure 1.15). This is not always true; instead, it depends on the choice of n_o. Let's simplify the concept by analyzing the number of paths from n_{in} to n_o with the same *mMd* from a 2D to a 3D lattice grid. In the 2D case we pose *mMd* = $X' + Y'$, in the 3D case *mMd* = $X + Y + Z$. Since we want *mMd* to be the same, it must be $X' + Y' = X + Y + Z$. In a 2D grid (10×10) let be (n_{in}, n_o) of coordinates [(1,1) ; (3,4)], it follows *X*= 3 - 1 = 2, *Y* = 4 - 1 = 3, and *mMd*= 3 + 2 = 5. By applying the eq.(1.2.5) in 2D, we can calculate the number of path with *mMd*=5 as:

$$P' = \frac{(X'+Y')!}{X'!\,Y'!} = \frac{5!}{12} = 10$$

In the 3D grid ($10 \times 10 \times 10$) we assign to n_{in} the coordinates (1,1,0). Depending on the choice of n_o, the number of paths with the same *mMd*=5 will change. For n_o of coordinates (2,2,3), in fact, we have *X,Y,Z*=(1,1,3), *mMd*=1+1+3=5, and the number of paths is:

$$P = \frac{(X+Y+Z)!}{X!\,Y!\,Z!} = \frac{5!}{1!\,1!\,3!} = 20$$

In this case, the number of paths in 3D increased consistently, but if we had chosen n_o of coordinates (0,1,4), we would have:

$$P = \frac{(X+Y+Z)!}{X!\,Y!\,Z!} = \frac{5!}{0!\,1!\,4!} = 5$$

which shows fewer paths compared to the 2D case (P'=10). Therefore, the choice of n_o would affect the number of paths which influences the *SGE* effect. We propose, hence, a way to determine the coordinates of n_o such as to benefit the *SGE*. Let's define the ratio α=*P*/*P*′, and consider $X' + Y' = X + Y + Z = mMd$. We want to find the coordinates of n_o such that $\alpha > 1$, which means $P > P'$, i.e., the number of paths in 3D are greater than those in 2D with the same *mMd*. Since $X + Y + Z = X' + Y' = mMd$ we can write:

$$\alpha = \frac{P}{P'} = \frac{(X+Y+Z)!}{X!\,Y!\,Z!} \times \frac{(X'!\,Y'!\,)}{(X'+Y')!} = \frac{(X'!\,Y'!\,)}{X!\,Y!\,Z!}$$

For $\alpha > 1$:

$$\frac{(X'!\,Y'!\,)}{X!\,Y!\,Z!} > 1 \rightarrow Z! < \frac{(X'!\,Y'!\,)}{X!\,Y!}$$

It follows:

$$\begin{cases} X + Y + Z = mMd \\ \\ Z! < \frac{(X'!Y'!)}{X!Y!} \end{cases} \tag{1.2.6}$$

Let's clarify everything with an example by using the same coordinates in 2D for (n_{in}, n_o) = [(1,1) ; (3,4)]. We know *mMd*=5, P'=10, X'=2, and Y'=3. We now choose some values for *X, Y* and calculate *Z* since we know *X+Y+Z=mMd*. Consequently, we just need to verify if *Z* satisfies the eq.(1.2.6). For instance, if we chose the values for (*X,Y*)=(1,2), we have *Z*=2, which satisfies eq.(1.2.6):

$$\begin{cases} X + Y + Z = mMd \\ \\ Z! < \frac{(X'!Y'!)}{X!Y!} \end{cases} \rightarrow \begin{cases} 1 + 2 + 2 = 5 \\ \\ 2! < \frac{(2'!3'!)}{1!2!} \end{cases}$$

Therefore (X,Y,Z)=(1,2,2) solves for $\alpha > 1$, and by substituting (1,2,2) in eq.(1.2.5), we expect to have $P > P'$:

$$P = \frac{(X + Y + Z)!}{X!\,Y!\,Z!} = \frac{5!}{1!\,2!\,2!} = 15 > P' = 10$$

From the eq.(1.2.2, 1.2.3, 1.2.4), by knowing [n_{in}:(1,1,0)] and [(X,Y,Z)=(1,2,2)] we can calculate 2 points for n_o =[$n_{o,1}$: (0,3,2); $n_{o,2}$:(2,3,2)]. The points have both *mMd*=5 to n_{in}:(1,1,0) whose number of paths is P= 15, greater than the number of paths P'=10 for 2 points having *mMd*=5 in the 2D network. Hence, by carefully choosing the coordinates of the n_o ($n_{o,1}$ or $n_{o,2}$), we can strengthen the *SGE* in the 3D network.

Let's evaluate two cases.

- ***A***: All distances are equals X=Y=Z, it follows:

  $$P = \frac{(3X)!}{(X!\,)^3} > 1$$

  Since the fraction is bigger than 1, for $n \rightarrow \infty$, considering the distances all equals, we have:

  $$P = lim_{n\rightarrow\infty} \frac{(n \times X)!}{(X!\,)^n} \rightarrow \infty$$

  .

- ***B***: In the 3D case where the distances are not equal, we can assume there is a minimum between them. For instance, let's be $X < Y < Z$ (the order is not relevant). We can develop eq.(1.2.5) by expressing Y, Z in the function of X. Since $X, Y, Z > 0$ we can write $Y = X + A$ and $Z = X + B$, with $0 < A < B$. We can write eq.(1.2.5) as:

$$P = \frac{[(X+B)+(X+A)+X]!}{(X+B)!\,(X+A)!\,X!} = \frac{[3X+B+A]!}{(X+B)!\,(X+A)!\,X!}$$

The numerator can be developed in 3 terms : $N = S \times L \times R$:

$$S = \underbrace{(3X+B+A)\cdot\cdot(3X+A+1)}_{B_{terms}} \;;\; L = \underbrace{(3X+A)\cdot\cdot(3X+1)}_{A_{terms}} \;;\; R = \underbrace{(3X\cdot\cdot X!\,)}_{3X_{terms}}$$

The denominator can be developed in 3 terms as: $D = S' \times L' \times R'$

$$S' = \underbrace{(X+B)\cdot\cdot(X+1)}_{B_{terms}} \;;\; L' = \underbrace{(X+A)\cdot\cdot(X+1)}_{A_{terms}} \;;\; R' = \underbrace{(X!\,X!\,X!\,)}_{3X_{terms}}$$

Let's consider the fraction N/D by comparing the fractions of the *B, A, 3X*$_{terms}$.

$$B_{terms} = \frac{S}{S'} \;;\; A_{terms} = \frac{L}{L'} \;;\; 3X_{terms} = \frac{R}{R'}$$

All the 3 fractions are greater than 1. If we increase the dimension *n, P* can be written as sum of *n* fractions all greater than 1, and for $n \to \infty$:

$$P = lim_{n\to\infty} \sum_{i=1}^{n} \frac{T_i}{T_i'} \to \infty$$

In any case, by increasing the dimension *n*, *P* increases.

1.2.2 Spiking activity

Single spike propagation

To gain a deeper understanding of the process time τ, we conducted a simulation in a 3D lattice grid network consisting of ($7 \times 7 \times 7$) identical RS neurons. The graphical representation in Figure 1.16 illustrates a simulation spanning 1000 milliseconds during which a solitary spike traverses the quickest route from the input neuron n_{in}:12 to the output neuron n_o:155 (with each neuron's number corresponding to its position in the grid). In this simulation, an initiating neuron emits a single spike at time $t = t_0$, which in turn stimulates its neighboring neurons. This action generates post-synaptic spikes that transform into pre-synaptic signals transmitted to adjacent neurons, and the process continues to propagate across the grid.

By categorizing all impulses with positive membrane potential in Figure 1.16 as "spikes," we observe that the second spike (occurring at the first post-synaptic neuron 61) occurs approximately at 100 milliseconds. Subsequently, the adjacent neuron 154 spikes around 110 milliseconds. The initial spike does not propagate entirely to the six adjacent neurons; instead, its potential fragments into smaller post-synaptic potentials (PSPs) that spread along the interconnected neurons in the system. A single neuron can be influenced by up to six PSPs, each arriving at approximately the same time, and eventually trigger a spike (as indicated by the green dot).

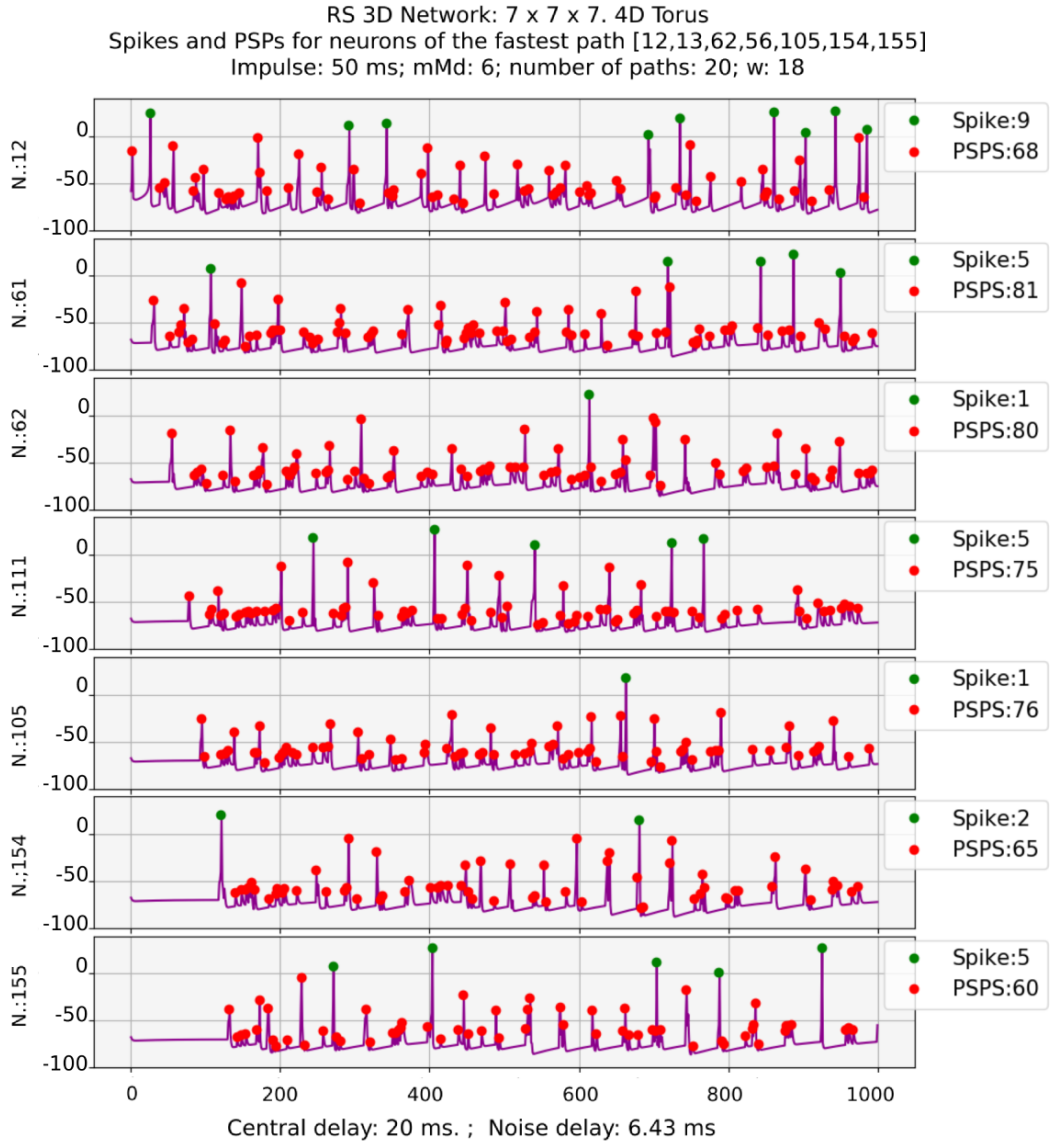

Figure 1.16: The membrane potential (vertical axis) of 6 adjacent neurons representing the propagation of a single spike in a 2D network of regular spiking (RS) Izhikevich neurons. The central delay is 10 with a noise of 6.43 ms, meaning the transition time μ varies in the range (13.57;26.43) ms. The plot shows the behavior and development of the single-impulse spike (green dot) from the initiator neuron n_{in}=12 across the path [12,61,62,111,105,154,155], with 155 being the output neuron n_o. We can observe how the initial spiking activity at neuron 12 induces connected neurons to spike after a brief delay of duration near the average axonal delay value (cd=20 milliseconds in the simulation shown).

Remarkably, a single impulse spike has the capacity to propagate and generate significant action potentials throughout the entire network within a 1000-millisecond timeframe.

RS vs Heterogeneous model

In this study, we investigate and compare the correlation between the randomness of neuron types and the average number of spikes that occur in the entire network over a specific duration. Initially, we examine homogeneous and heterogeneous models using a 3D model (4D torus). We conduct multiple simulations while varying the level of heterogeneity from 0 to 1. A heterogeneity level of 0 signifies that all neurons are of the same type (RS Izhikevich), while a level of 1 represents a completely heterogeneous network of Izhikevich neurons, as defined in reference [29]. In all these simulations, a constant current of 10 mA triggers the input (initiator) with n_{in} set to 12. It's important to note that increasing axonal delay and heterogeneity accelerates the propagation of spikes, leading to a logical expectation that the number of spikes will rise as heterogeneity increases. In contrast, an examination of Figure 1.17 uncovers an unexpected phenomenon, where the occurrence of spikes decreases as the level of variability increases. The plot depicts the results of 15 different simulations, each lasting 1000 ms, conducted at six different levels of heterogeneity. In each simulation, the central delay is held constant at 22 ms, while δ^i ranges from 0 to 20 ms. The first simulation provides the average number of spikes in the network with a central delay of 22 ms and a maximum variability of 0 ms. In this scenario, all neurons exhibit the same transition time, with μ equal to 22 ms. Furthermore, since all neurons are of the RS type, their processing time for action potential signals, denoted as τ, is approximately uniform. In Figure 1.16, assuming constant values for μ and τ, we observe a smooth synchronization of signals in the network. This synchronization implies that signals, such as s_1, s_2, and s_3 in Figure 1.15(b), are likely to reach n_o simultaneously, given the constancy of μ and τ. This synchronization results in the PSPs clustering together at approximately the same time, leading to the generation of spikes.

On the contrary, when the level of stochastic variation in axonal delay amplifies, the transmission time, denoted as μ, exhibits fluctuations as described in equation (1.1.2). As a result, the synchrony of signals diminishes, causing them to reach their destination with varying time intervals, thereby diminishing the probability of postsynaptic potentials (PSPs) converging to generate a neuronal spike. As the degree of noise escalates, the level of synchronization decreases, whereas the incidence of spike occurrences rises.

Surprisingly, it is evident that as axonal heterogeneity value changes, the spiking activity of the network maintains a consistent shape (see Figure 1.17) for all values of neural heterogeneity. To elaborate, while the heterogeneous axonal delay primarily influences the spatial separation between neurons, neural heterogeneity is fundamentally associated with the neuron model, affecting the variability in τ specifically, how distinct neurons process pre-synaptic signals with varying *process time*.

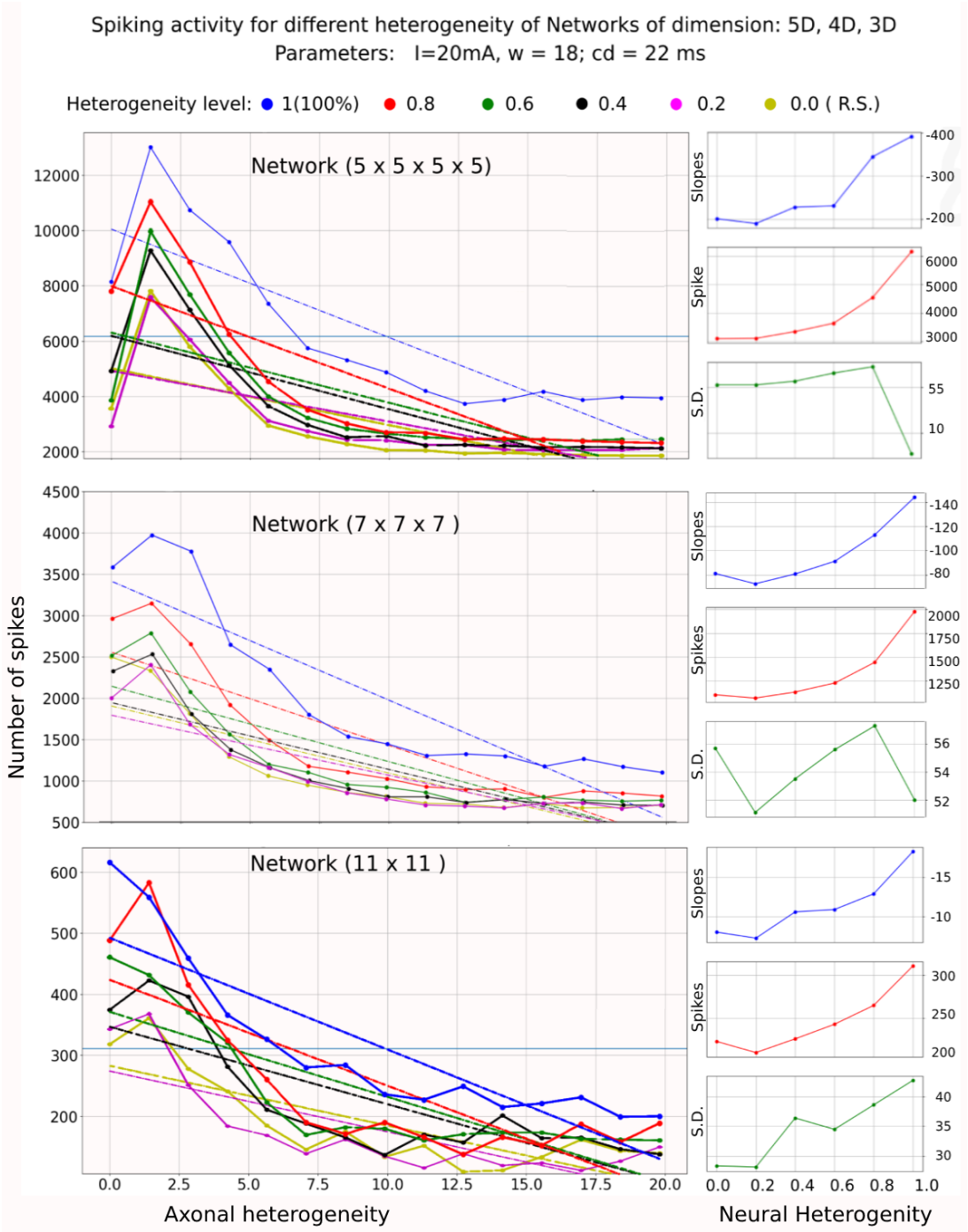

Figure 1.17: The study investigates the relationship between axonal delay randomness, which ranges from 0 to 20 milliseconds, and the number of spikes. This analysis focuses on a central delay of 22 milliseconds and encompasses six different levels of neuronal heterogeneity across three distinct network dimensions. The count of spikes and the associated standard deviation are computed across hundreds of neurons, and the outcomes are influenced by the network's size. The graph illustrates the results, with a blue dot (1) representing complete heterogeneity and a yellow dot (0.0) symbolizing zero heterogeneity (all RS neurons). Across all three networks, the number of spikes for H=1.0 is approximately twice as high as that for H=0.0. It's worth noting that as spatial variability increases, the number of spikes decreases, and this effect is more pronounced in models with higher levels of heterogeneity. The right-hand panels display the linear regression coefficients (top) for the six heterogeneity levels, ranging from 0.0 to 1.0. The central values show the mean number of spikes for each level of heterogeneity (center) and the corresponding standard deviation (bottom).

Nt.size		H.:0.0	H.:0.2	H.:0.4	H.:0.6	H.:0.8	H.: 1.0
$5 \times 5 \times 5 \times 5$	S.D.	55.3	55.3	55.7	56.6	57.7	47.7
	Mean	3091	3101	3340	3636	4543	6166
	Slope	-201	-190	-228	-231	-345	-392
$7 \times 7 \times 7$	S.D.	55.7	51.1	53.5	55.6	57.3	52
	Mean	1104	1069	1133	1228	1445	1978
	Slope	-81.2	-72.7	-80.0	-91.3	-113	-144
11×11	S.D.	28.4	28.2	36.4	34.5	38.6	42.7
	Mean	223	210	226	243	265	311
	Slope	-8.02	-7.25	-10.6	-10.9	-12.9	-18.3

Table 1.2: The table summarizes the data of figure 1.17. For each of the three networks are specified the value of standard deviation (S.D.), the average number of spikes of the network (Mean), and the interpolation line (Slope) for all the heterogeneity values (from H:0.0 to H:1.0)

1.3 Network partitioned in equivalence classes.

1.3.1 *mMd* induces equivalence classes on the network: Octahedrons.

We commence by partitioning the network based on the equivalence relationship denoted as *mMd*. This process results in the formation of neuron groups that share similarities in their connections and characteristics, facilitating the subsequent examination of the network by scrutinizing these groups. To begin, we revisit the definitions of *equivalence classes* and the *equivalence relationship*, as presented by ϕ [47] within the context of a given set *F*. A relation ϕ defined on a set *F* is classified as an equivalence relation if and only if it satisfies three essential criteria:

1. It is *reflexive*: for any $a \in F$, *a* must be equivalent to itself: $a \ \phi \ a$
2. It is *symmetric*: For any couple (*a,b*) $\in F$, if $a \ \phi \ b \rightarrow b \ \phi \ a$
3. It is *transitive*: Let *a, b, and c* $\in F$.

   Then, if $a \ \phi \ b$ and $b \ \phi \ c \rightarrow a \ \phi \ c$

If ϕ is an equivalence relationship on *F*, we can define the equivalence classes on *F* as:

$$[a] = \{x \in \ F \mid x \ \phi \ a\}$$

It can be shown that any two equivalence classes are either equal or disjoint, hence the collection of equivalence classes forms a partition of *F*, called *quotient set* of *F*, indicated as $\overline{F}$, divided into non-empty subsets, in such a way that every element of *F* is included in exactly one subset of $\overline{F}$ [48]. The quotient set is defined as:

$$F/\phi = \overline{F} = \{[a] \mid a \in \ F\} \tag{1.3.1}$$

Hence, we build the same mathematical structure in the network by proving *mMd* to be an equiv-

alent relationship in *Nt*. This induces a quotient set of equivalence classes on it. We randomly choose a neuron n_{in} as the initiator. We consider the neurons $n_i,\ n_j$ to be in relationship ϕ, $n_i\ \phi\ n_j$, if they have the same ***mMd*** to n_{in}. We refer to ***mMd*** for n_{in}, as the minimum number of steps to reach n_{in} from a node n_j, as explained in figure (1.18). In order for ϕ to be an *equivalence relationship* on *Nt* we need to prove the following three points:

- *reflexive*: $\forall\ n_i \in Nt\ \rightarrow n_i\ \phi\ n_i$.

  The reflexivity here is trivial since ϕ is an equality relationship. If n_i has ***mMd*** to n_{in} it is obviously in a relationship with itself.

- *symmetric*: $\forall\ n_i, n_j \in Nt$ if $n_i\ \phi\ n_j\ \rightarrow n_i\ \phi\ n_j$
  For any couple of neurons $n_i, n_j \in Nt$, if $n_i\ \phi\ n_j$, it means n_i, n_j have the same ***mMd*** to n_{in} for the commutative property of equality relationship it follows $\rightarrow n_j\ \phi\ n_i$.

- *transitive*: $\forall\ n_i, n_j, n_k \in Nt$:
  if $n_i\ \phi\ n_j$ *and* $n_j\ \phi\ n_k \rightarrow n_i\ \phi\ n_k$.
  If $n_i\ \phi\ n_j \rightarrow n_i$ and n_j have the same ***mMd*** to n_{in}. If and $n_j\ \phi\ n_k \rightarrow n_j$ and n_k have the same ***mMd*** to n_{in}. From the transitivity properties of equality, it simply follows n_i and n_k have the same ***mMd*** to n_{in}, that is to say, $n_i\ \phi\ n_k$.

Therefore, given a random n_{in}, ϕ is an *equivalence relationship* on *Nt* inducing *equivalence classes* of the form:

$$[n_{in}^m] = \{n_i, n_j \in Nt \mid n_i\ \phi\ n_j\},\ \text{with: } 1 \leq m \leq g \tag{1.3.2}$$

where *g* is the maximum ***mMd*** from n_{in}. There would be, hence, *g* equivalence classes described in eq.(1.3.2).

In Figure 1.18, the neurons belonging to a class denoted as $[n_{in}^m]$ are positioned along a geometric structure that can be described as an "octahedron." These classes take their names from the shape itself. The class $[n_{in}^m]$ encompasses all neurons n_j that share the same ***mMd*** value as the initiating neuron n_{in}. The quotient set Nt/ϕ serves as a valid partition of the set Nt and represents the collection of all octahedrons. These octahedrons possess the properties of having non-overlapping intersections (meaning that a neuron *n* cannot be part of more than one distinct octahedron) and collectively forming the entirety of the set Nt.

1.3.2 Statistical entropy: macrostate and microstate.

Statistical entropy holds significant relevance within the domain of statistical mechanics. As expounded by Boltzmann's research [49], entropy can be construed as a quantification of the multitude of conceivable microscopic states (microstates) from which a given macrostate of a system may emerge [50]. If we denote Ω as the count of microstates contributing to the realization of a specific macrostate denoted as *A*, then, in accordance with Boltzmann's equation, the likelihood of this particular macrostate manifesting is directly proportional to the value of Ω:

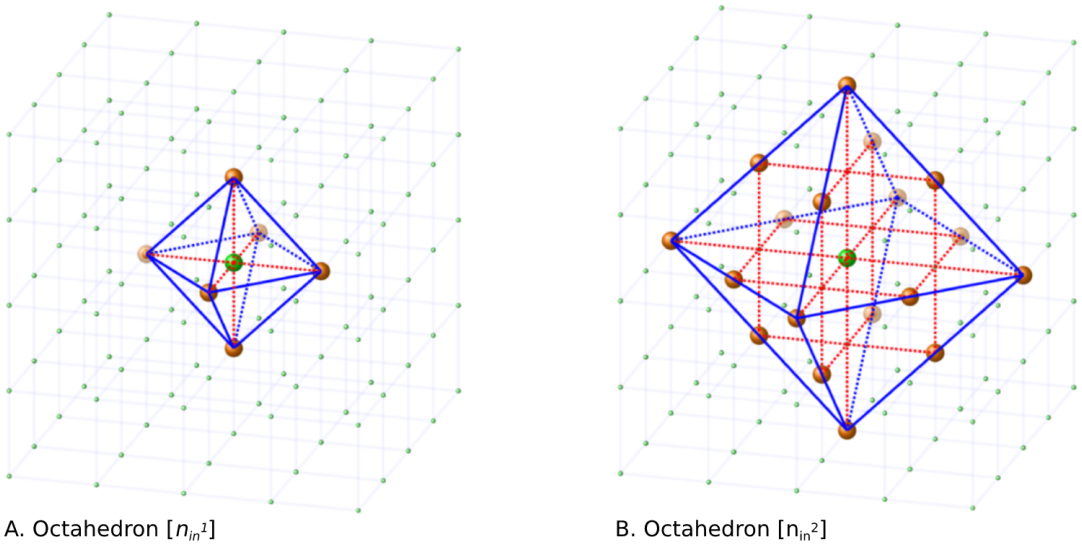

Figure 1.18: An illustration featuring the *mMd* and the corresponding equivalence classes $[n_{in}^1]$ and $[n_{in}^2]$ is presented. The central green node represents the initiator neuron, denoted as n_{in}. In Figure **A**, we depict the class $[n_{in}^1]$, comprising a collection of six neurons, all with a *mMd* value of 1 with respect to n_{in}. The *mMd* is represented by a red dotted line. In Figure **B**, we turn our attention to the class $[n_{in}^2]$, which consists of eighteen neurons, each having an identical *mMd* of 2, measured from the same reference neuron, n_{in}. The red dotted lines in this context illustrate the paths required to reach n_{in} in exactly two steps. These sets are comprised of 18 elements, all maintaining equivalent relationships with each other. Hypothetically connecting these nodes would result in the neurons lying on the surface of an octahedron.

$$S(A) = ln_2(\Omega) \tag{1.3.3}$$

We have chosen to omit the inclusion of Boltzmann's constant in the current context, as it proves unnecessary for the purposes of our study; nonetheless, it has been computed in the course of our simulation. The function under consideration quantifies the total number of feasible arrangements for a given macrostate. The quantity denoted as *S(A)*, corresponding to the entropy of macrostate *A*, serves as a measure of the information required for describing the system. The probability of encountering the system in a particular state, or macrostate, hinges upon the microstates that compose that specific macrostate; in other words, it is directly proportional to the count of possible microstate configurations. To elucidate this relationship among microstates, macrostates, and entropy, we offer an illustrative example related to equation (1.3.3). When rolling two dice, the microstate associated with macrostate *A=2* is singular, while the number of microstates for macrostate *A=7* amounts to six, reflecting the six distinct combinations of dice that result in a total of seven pips. As depicted in Figure (1.19), the macrostate with the highest likelihood of occurrence, or, equivalently, the highest entropy, is macrostate *A=7*, characterized by an entropy of $S(7) = \ln(6)$. This observation aligns with the fundamental principle that the macrostate possessing the greatest number of microstates corresponds to the macrostate with the highest entropy

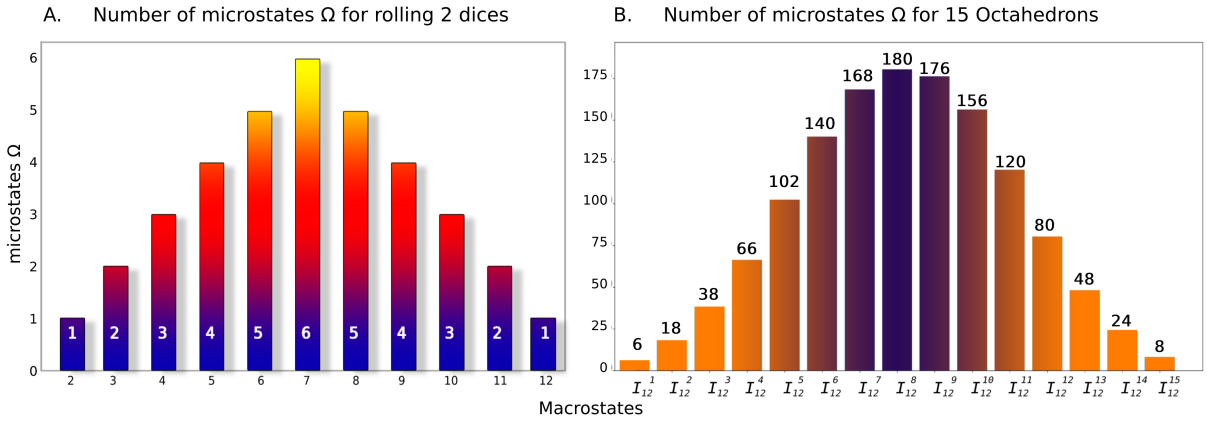

Figure 1.19: In panel A, the system can assume one of the eleven possible macrostates from 1 to 12 on the *x-axes*. The macrostate *7* is the one with the highest probability to happen since it has the greatest number of microstates $\Omega = 6$, *y-axes*. Therefore, it is the macrostate with the highest entropy and the most likely state the network will tend to.
In panel B, the picture represents the number of microstates for the macrostate of a network of ($11\times$ 11×11) neurons. For the initiator neuron n_{12}, *mMd* assumes values from 1 to 15, formulating fifteen *octahedrons* and, therefore, fifteen macrostates. According to eq. (1.3.3) the macrostate with the highest entropy is the macrostate I_{12}^{8} with 180 microstates whose entropy is $S(I_{12}^{8}) = log(180)$.

1.3.3 Macrostate and microstate of octahedrons: interspike train.

In the previous sections, denoted as 1.3.1 and 1.3.2, we have provided definitions for octahedrons as equivalence classes within the network and statistical entropy in terms of microstate and macrostate. Our objective now is to incorporate these concepts into our network framework. Firstly, we should revisit the concept of interspike training, which pertains to the time intervals between successive action potentials (also known as spikes) of a neuron within a period denoted as T. An interspike train is represented by n_{in} and encompasses the activities of other neurons in the network after the time T has transpired. Given our division of *Nt* into *g*-octahedrons $[n_{in}^{m}]; (1 \leq m \leq g)$, we designate I_n as the interspike train of neuron $n \in [n_{in}^{m}]$. Additionally, we define the interspike train of the octahedron $[n_{in}^{m}]$ as the union of the interspike trains I_n, denoted as $I_{n_{in}}^{m} = \bigcup I_n \mid n \in [n_{in}^{m}]$. $I_{n_{in}}^{m}$ signifies the collection of interspike frequencies, or spiking activity, within the octahedron $[n_{in}^{m}]$, representing a possible state of network activity after the time T. $I_{n_{in}}^{m}$ constitutes a macrostate, representing a potential configuration of spiking activities within *Nt*. Consequently, octahedrons with a larger number of neurons are expected to exhibit more substantial spiking activity compared to those with fewer neurons. Thus, they are more likely to approximate network spiking activity over a simulation period T. Once we have linked each octahedron $[n_{in}^{m}]$ to its respective macrostate $[I_{n_{in}}^{m}]$, we need to establish the concept of microstates Ω. To simplify the concept and facilitate calculations, we can proceed as follows. Since a microstate within $[I_{n_{in}}^{m}]$ corresponds to the interspike train I_n generated by a single neuron *n*, the macrostate with the highest number of microstates is associated with the octahedron $[n_{in}^{m}]$ that has the most neurons. If an octahedron possesses a greater number of neurons, its associated macrostate $I_{n_{in}}^{m}$ will have a larger number of interspike trains (microstates) I_n. Consequently, as the number of neurons in an octahedron increases, its entropy also increases. The cardinality of an octahedron can be employed to represent the number of microstates. Finally,

in accordance with equation (1.3.3), we can express this as follows:

$$S([I_{n_{in}^m}]) = ln(\mathbf{card}([n_{in}^m])) \tag{1.3.4}$$

Where:

- $S([I_{n_{in}^m}])$ = the entropy of $I_{n_{in}}^m$ (octahedron $[n_{in}^m]$).
- $\Omega = \mathbf{card}([n_{in}^m])$.

As in figure 1.19 panel B, for *Nt* = $(11 \times 11 \times 11)$ with $n_{in} = 12$, the macrostate $I_{n_{12}}^8$ has the highest entropy and we expect it to best approximate the interspike distribution (spiking activity) of the network *Nt*. Given the toroidal shape of the models, we can estimate the octahedron with the highest number of neurons as that one formed by a *mMd=g/2*, where *g* is the maximum *mMd*.

We refer to such distance as ζ: where:

$$\begin{cases} \zeta = (g/2) + 1\textit{; if g is an even number} \\ \zeta = (g+1)/2\textit{; if g is an odd number} \end{cases} \tag{1.3.5}$$

We refer to the octahedron n_{in}^{ζ} as the class with the macrostate $I_{n_{in}}^{\zeta}$ with the highest entropy.

1.3.4 Shannon entropy

The mathematical representations of entropy as formulated by Boltzmann and Gibbs exhibit similarities with Shannon's concept of information entropy, which was developed during the 1940s [51]. Gibbs entropy, which pertains to the probability distribution of microstates, serves as a generalization of Boltzmann's entropy [52]. It serves to quantify the extent of disorder or randomness within a physical system. In a parallel vein, Shannon entropy, also referred to as information entropy, provides a metric for the average information content or uncertainty associated with a random variable. The computation of Shannon entropy is expressed as follows:

$$H(X) = -\sum_{i}^{n}[p_i(x) \times log_2(p_i(x))] \tag{1.3.6}$$

The logarithm base 2 results in entropy measurements in bits [53]. It is maximum when all possible outcomes are equally likely (a uniform probability distribution). It is zero when there is only one possible outcome (a deterministic distribution). In the context of neuron activity, Shannon entropy can be used to quantify the level of information or variability in neurons' firing patterns within a population. To calculate the Shannon entropy of neuron activity, we would first discretize the ISI distribution of the neurons in each octahedron. Then, we can compute the probability distribution of spike occurrences during the simulation time *T* by counting the number of spikes in that interval and normalizing it by the total number of spikes observed. Once

we obtain the probability distribution, we can calculate the Shannon entropy using the formula:

$$H = -\sum(p([n_{in}^i]) \times log_2(p([n_{in}^i]))) \tag{1.3.7}$$

The p_i represents the probability of spike occurrence in the octahedron $[n_{in}^i]$. A higher Shannon entropy value indicates a more diverse or unpredictable firing pattern. This suggests a larger amount of information contained in neuronal population activity. Conversely, a lower entropy value implies a more regular or predictable firing pattern [54].

Chapter 2

Chapter 2: Results

2.1 Strengthening of the *SGE* effect.

We now compare the evidence of the *SGE* effect on three different networks and confirm the mathematical formulation expressed in eq.(1.2.5). To verify the SGE effect from one dimension to another, the choice of n_{in} and n_o must be done accordingly. As pictured in figure 1.15, in panel (b) we chose n_o to be in a different plane than its counterpart in panel (a), where, even if the *mMd* is 3 in both cases, the number of paths duplicates in the 3D grid model. We consider three network grids (2D, 3D, and 4D) of regular firing (RS) neurons. First, we examine the simulation's spike timing data. Depending on the dimension of the model, the heterogeneous spatial structure of the grid reduces the time of propagation of spiking information.

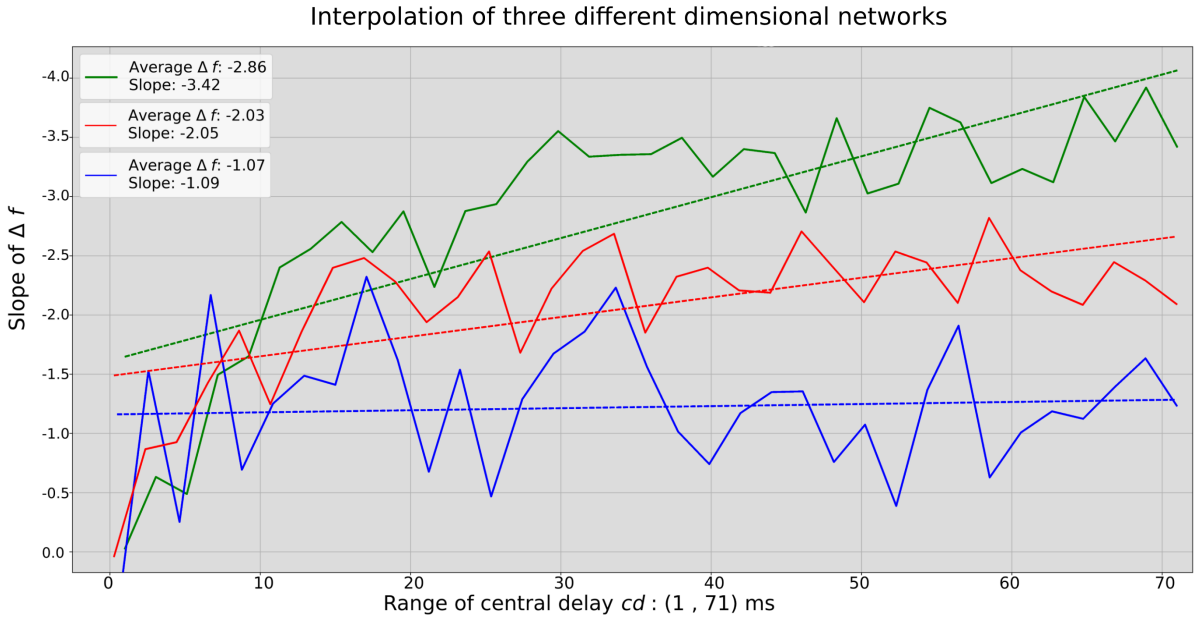

Figure 2.1: Comparison of regression slopes for three-dimensional toroidal networks in 3D (blue), 4D (red), and 5D (green). The simulations show the variation of the central delay $(cd)_j$ from 1 to 71 msec in 2 msec steps. For each delay value, we executed 40 simulations. By changing the grid's spatial randomness, we measure the first spike's arrival time. These 40 values are linearly interpolated, and the negative value of the slope reveals the SGE effect; in other words, it shows that the interval between the first spike of n_{in} and the first output of n_o decreases as the spatial heterogeneity of the grid increases. In all three models the n_{in} is subjected to the same current I=10 mA. All the neurons in the network have synaptic strength w=18. We used the Izhikevich model implemented in pyNest. For each network grid (2D, 3D and 4D), we chose (n_{in}; n_o) to have the same Manhattan distance *mMd*. By maintaining the same *mMd* and increasing the network dimension, the number of paths with the same *mMd* will increase and strengthen the SGE effect.

We changed the intrinsic axonal delay $(cd)_j$ from 1 up to 71 milliseconds and tested twenty different levels of noise delay $(nd)_i$ for each $(cd)_j$. In figure 2.1 we compare the regression

T.D.	Nt. size	I	w	n_{in}	n_o	*mMd*	Paths	Slope
3D	11×11	10	18	12	116	6	6	-1.09
4D	7×7×7	10	18	12	155	6	20	-2.05
5D	5×5×5×5	10	18	12	296	6	180	-3.42

Table 2.1: The characteristics of the multidimensional neural networks used in the simulations reported in figure 2.1

OCTAHEDRONS															
Octahedron	$[n_{12}^1]$	$[n_{12}^2]$	$[n_{12}^3]$	$[n_{12}^4]$	$[n_{12}^5]$	$[n_{12}^6]$	$[n_{12}^7]$	$[n_{12}^8]$	$[n_{12}^9]$	$[n_{12}^{10}]$	$[n_{12}^{11}]$	$[n_{12}^{12}]$	$[n_{12}^{13}]$	$[n_{12}^{14}]$	$[n_{15}^{12}]$
Cardinality	6	18	38	66	102	140	168	180	176	156	120	80	48	24	8
Spike	136	364	752	1257	1811	2544	2988	3162	2994	2633	1964	1309	788	403	155

Table 2.2: Display of the data of the histograms in figure 2.2. For each octahedron, 'Cardinality' represents the number of neurons that belong to the octahedron, while 'Spike' represents the number of spikes within the corresponding octahedron. The class $[n_{12}^1]$ has 6 elements that perform 136 spikes during simulation time *T*.

coefficient for the delay difference time Δf in the case of three different networks: 3D, 4D, and 5D. Every single point of a line represents the slope resulting from 20 simulations with a fixed central delay. The $(nd)_i$ varies from 0 to *cd*.

The negative value indicates a faster propagation of the signal. The three networks have the same initiator neuron n_{in} in position 12, driven by a constant 10 mA current. Across the whole network, all neurons are connected with constant synaptic strength $w = 18$. However, the output n_o has been chosen to have the same Manhattan distance *mMd* from n_{in} in all three different models. We notice that while the dimension increases, the number of paths increases according to (1.2.5). Respectively for the networks of 2D (Torus 3D), 3D (Torus 4D), and 4D (Torus 5D), n_o is set up to be at positions 116, 155, and 296. This results in 6, 20, and 180 paths with the same *mMd*=6, for each model. Noticeably, the average slope value decreases as the dimension rises, from -1.09 (3D Torus) to -2.05 (4D Torus) and -3.42 (5D Torus). Based on our discussion of equation 1.2.5, information propagates faster in higher-dimension networks. In other words, increasing the dimension increases the number of paths from n_{in} to n_o, and increases the number of spikes arriving at n_o, resulting in a higher probability for the *SGE* effect to occur.

2.2 Network entropy

We consider the equivalence relationship *mMd* on *Nt* which subdivides the network into octahedrons, equivalent classes. The partition of *Nt* in its quotient set $\overline{Nt} = Nt/mMd$, the set of all octahedrons, permits us to compare the system entropy with the entropy of every octahedron as the axonal heterogeneity (noise) increases. To do this we recall the functions of Boltzmann and Shannon, as well as the equations eq.(1.3.3) and eq.(1.3.6), to calculate the entropy for each octahedron and of the network. We compare the entropies of their respective interspike trains during their simulations and plot the results.

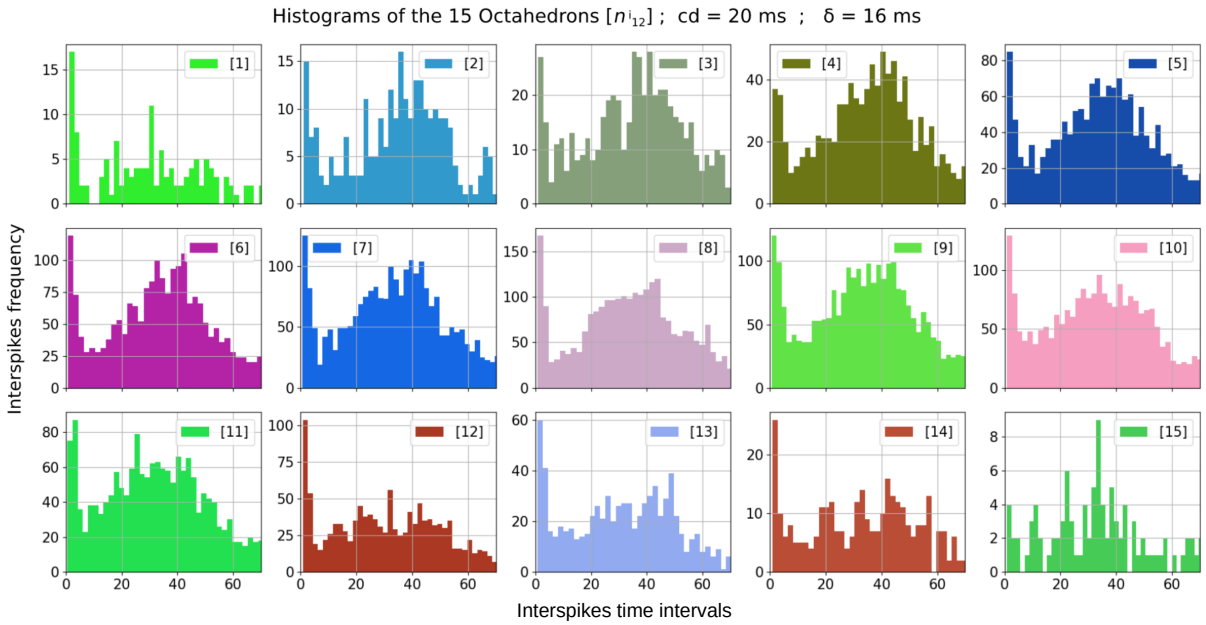

Figure 2.2: Illustration of the fifteen octahedrons of a network of size $11 \times 11 \times 11$ (1331 neurons) of full neural heterogeneity. The initiator neuron n_{in}=12 is supplied with a current of I= 10.0 mA and synaptic strength w=18. The network is subdivided into octahedrons (equivalence classes), according to the equivalence relationship *mMd* which ranges from 1 to 15. The number in the legend of each histogram represents the corresponding octahedron class. For instance, in the top left panel the number 1 stands for the octahedron $[n^1_{12}]$, and so on. The macrostate (octahedron in this case) with the highest entropy is the class $[n^8_{12}]$ (panel number 8), with a number of microstates =180 and entropy $S([n^8_{12}]) = ln(180)$, which we expect to best describe the network's entropy. The class with the highest entropy represents the macrostate towards which the network is most likely to move. As shown in the picture 1.19 and the data in table 2.2, the behavior of the macrostates' interspike frequency is proportional to their cardinality. Class $[n^8_{12}]$ has the greatest cardinality (180 neurons) and the strongest spiking activity.

Boltzmann entropy.

The equivalent relationship *mMd* induced on *Nt*, a quotient set whose classes are named *octahedron*. According to the analytical expectation of Boltzmann's equation for statistical entropy, the macrostate with the highest entropy is the one with the highest value of microstates. The macrostate of the system is defined as the set $I^m_{n_{in}}$ of the interspike trains of all of the neurons of the octahedron $[n^m_{in}]$ whose cardinality is the number of neurons of the octahedron itself. Consequently, by extrapolating the cardinality of each octahedron we can predict the macrostate with the highest entropy. This is, equivalently, the interspike-train distribution the system is most likely to assume. Given the toroidal shape of the model, we can estimate the octahedron with the maximum number of neurons as shaped by a *mMd*=ζ as in eq.(1.3.5).

Accordingly, we refer, respectfully, to $[n^\zeta_{in}]$ and $I^\zeta_{n_{in}}$ as the octahedron with the highest number of neurons and the macrostate with the highest entropy.

After running a number of simulations, we compare the results with analytical expectations. We have constructed a neural heterogeneous network of size $(11 \times 11 \times 11)$ with Izhikevich neurons in figure 2.2. The initiator neuron n_{in}=12 was connected to a constant I= 10.0 mA and synaptic strength w=18. Specifically, figure 2.2 depicts the study of the interspike train, spiking activity, for a central delay (*cd*) of 20 ms and noise delay (*nd*) of 16 ms. The maximum *mMd* (g) is

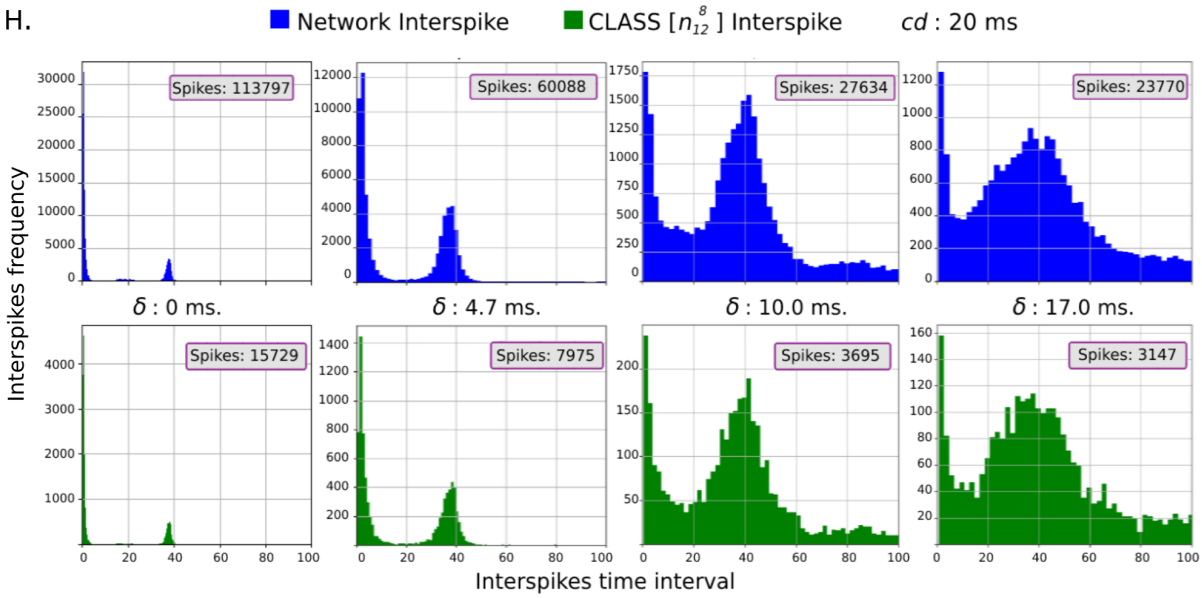

Figure 2.3: The plot refers to a heterogeneous neural network. Izhikevich's neurons are not identical. From the network described in figure 2.2, the top panel (blue) depicts the interspike frequency of the network, and the bottom panel (green) depicts the interspike frequency for the class $[n_{12}^{8}]$, the macrostate with the highest entropy. The histograms refer to four different simulations of time T: 1000 ms, where the heterogeneous axonal delay is calculated over a cd= 20 ms and four different values of the noise delay δ, respectively 0, 4.7, 10.0, and 17.0 ms. As each legend reports the number of total spikes, we can see that by changing δ, the interspike frequency distribution of the octahedron $[n_{12}^{8}]$ tracks that one of the networks. As δ increases, the interspike frequency distribution follows that of the network. This indicates that noise delay has a large impact on the overall activity of the octahedron.

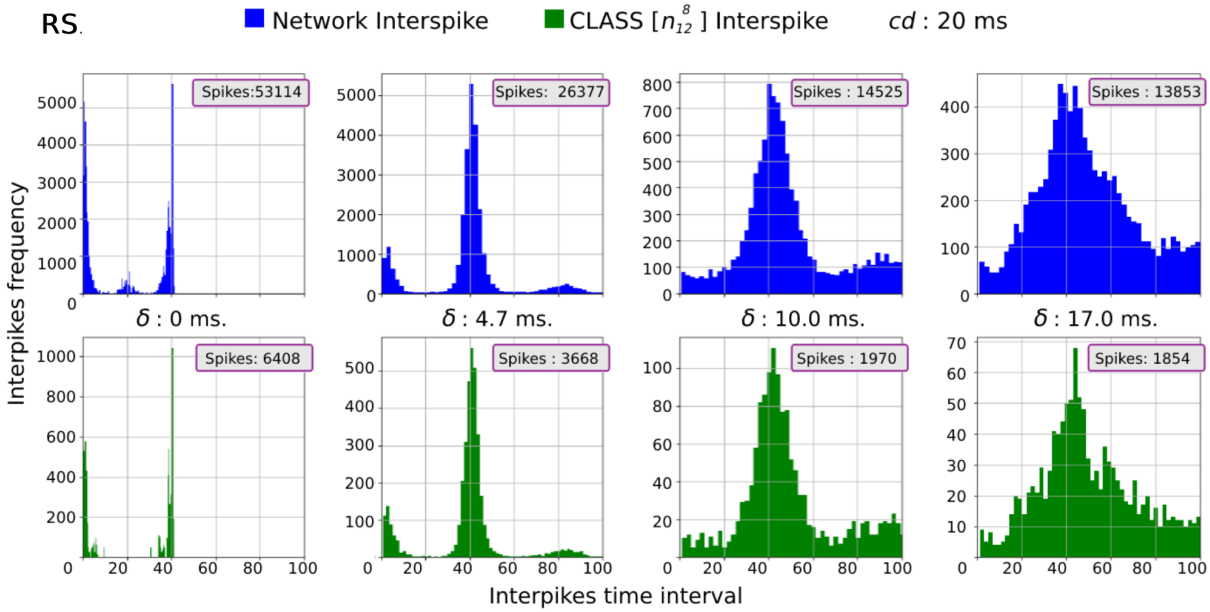

Figure 2.4: Similarly, in figure 2.3, we compare the frequency distribution of the class $[n_{12}^{8}]$, bottom panel (green), and of the network, top panel (blue). Neural homogeneity case. All neurons spike regularly (RS). Also in this situation, we observe that by changing δ, the interspike frequency distribution of the octahedron $[n_{12}^{8}]$ tracks the distribution of that network.

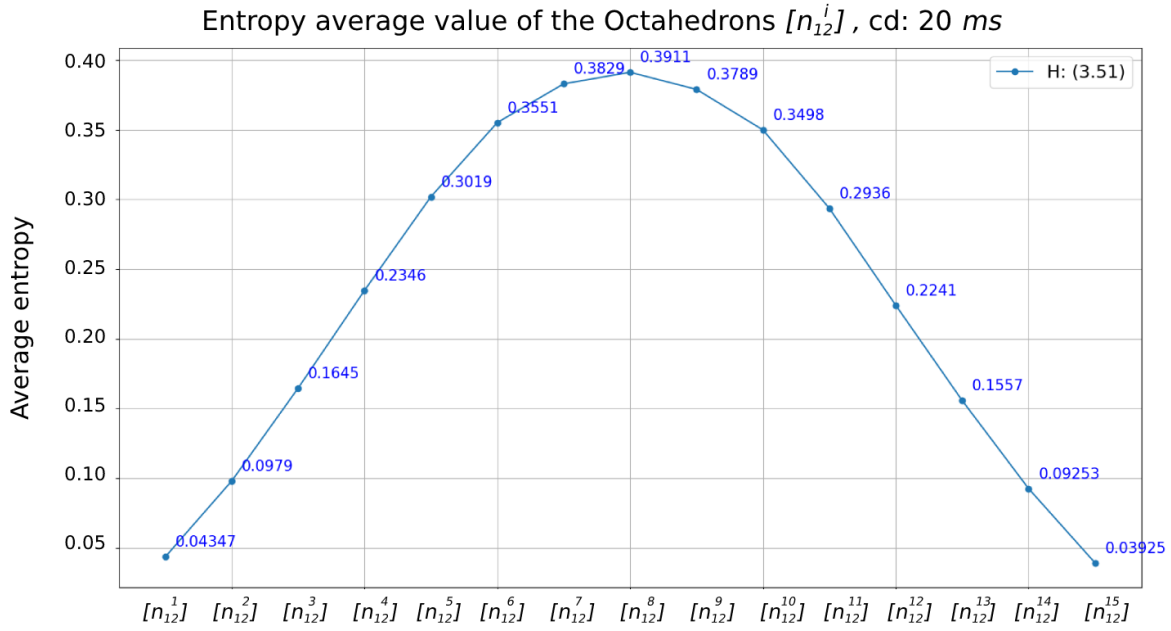

Figure 2.5: Heterogeneous neural network. The plot shows the distribution of the average entropy of the equivalent classes $[n_{12}^i]$ over 20 simulations for a cd=20 ms as the noise ranges from 0 to 20 ms. We determine the probabilities associated with each class, $p_i = p([n_{12}^i])$, and calculate their entropy, according to $H([n_{12}^i]) = -p_i \times log2(p_i)$. We take the average entropy for each class across the 20 simulations centered on a central delay of cd=20 ms. Each value is a term of the average entropy of the network of equation $H(X) = -\sum_i^n [p_i \times log_2(p_i]$ whose values are plotted in figure 2.6. We can observe how the highest value belongs to the class $[n_{12}^8]$, which has the highest number of neurons. Having the highest entropy means that the class exhibits the highest level of unpredictability/information content. In the legend, the value 3.51 is the average entropy of the network for a cd=20 ms noise range. It corresponds to the sum of the average entropies of the classes (plotted values).

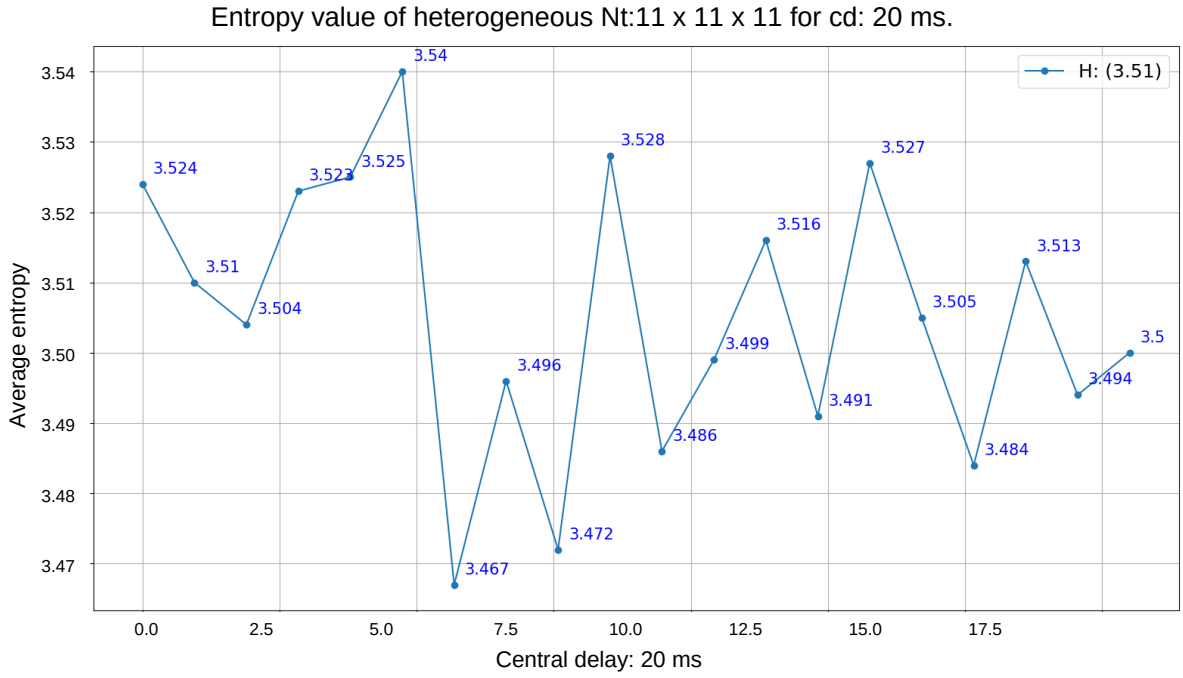

Figure 2.6: Heterogeneous neural network. As in figure 2.5, we consider the average entropy over 20 simulations for a cd=20 ms as the noise ranges from 0 to 20 ms. In this case, each value is the average value of the network's entropy. The legend reports a final average of 3.51, as we expect from figure 2.5.

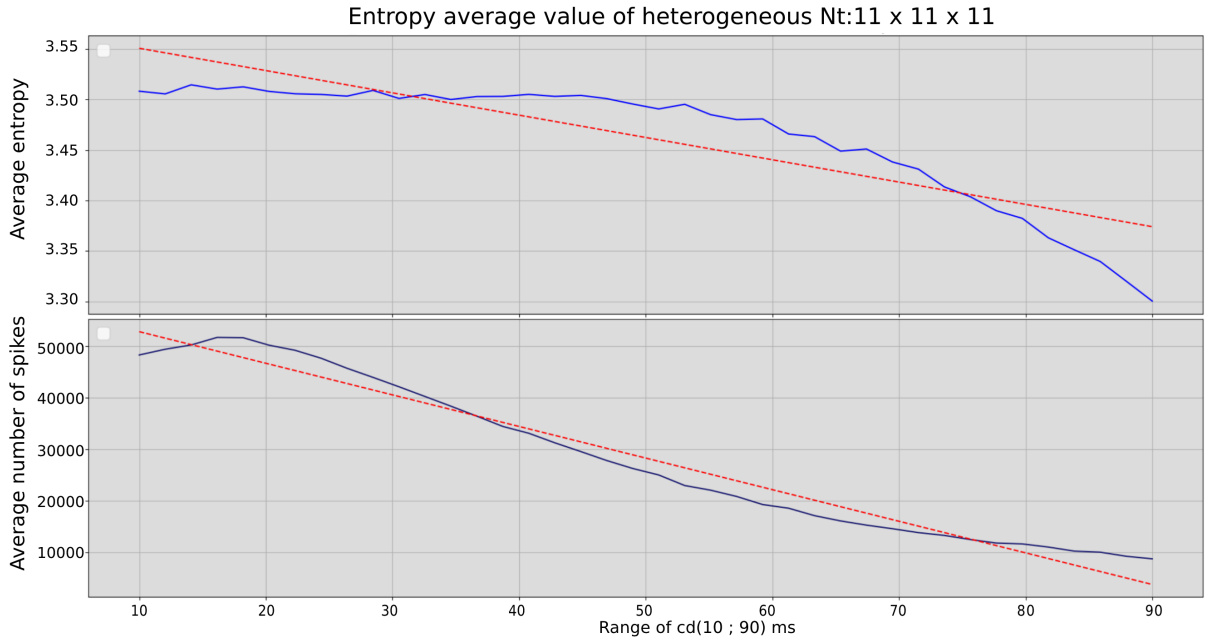

Figure 2.7: Heterogeneous neural network. The relationship between the network's average number of spikes and its average Shannon entropy is reported as the central delay *cd* ranges from 10 ms to 90 ms. For each *cd*, as in figure 2.6, we calculated the average value, both for the number of spikes and entropy, over 20 simulations as the noise ranges accordingly.

calculated as $[(ln/2) - 0.5] \times 3$. Since the side *ln*=11 and the network dimension is three, it follows *g*=15.

The quotient set $\overline{Nt}$, in this case, is subdivided into 15 octahedrons and ζ=8. Figure 2.2 depicts the interspike-train distribution during a simulation time *T*, for each of the fifteen octahedrons. Table 2.2 reports the number of neurons and the total number of spikes in every octahedron after a time *T*. We can observe how the interspike-train distribution varies by class and shows the maximum number of spikes in the octahedron $[n^8_{12}]$. The macrostate I^{ζ}_{12} of the octahedron $[n^8_{12}]$, is the one with the highest entropy. It shows a number of microstates =180 and entropy $S(I^{\zeta}_{12}) = ln(180)$.

We aim to conduct a comparative analysis of the interspike-train distribution of I^{ζ}_{12} with that of the network *Nt*. Figure 2.3 illustrates the interspike-train distributions for *Nt* (depicted in blue at the top) and the macrostate I^{ζ}_{12} (depicted in green at the bottom). This analysis is conducted under conditions of neural heterogeneity and involves four distinct values of axonal delay (noise) with a fixed value of *cd* equal to 20 ms. When altering the noise levels, both the interspike-train distributions for *Nt* and I^{ζ}_{12} exhibit proportional changes over time *T*. In Figure 2.4, we present the interspike-train distributions for the same axonal delay parameters, but within a homogeneous neural network, where all neurons follow the Izhikevich regular spiking (RS) pattern. In this scenario, the proportion of interspike-train distributions for both *Nt* and I^{ζ}_{12} remains relatively constant, irrespective of whether the number of spikes decreases significantly. Thus, even in a homogeneous system, the proportion of interspike-train distributions remains consistent, regardless of the level of noise. This observation suggests that while noise can enhance the

spiking activity of the system, it does not significantly impact the relative proportion ρ of the interspike-train distributions. This underscores the robustness of the subdivision of the system into octahedrons, maintaining stability even in the presence of noise. In both cases denoted as (**H**) and (**RS**), as anticipated based on the equation (1.3.3), the octahedron structure closely approximates the interspike frequency distribution of *Nt*. An analysis of the interspike frequency distribution reveals that in both cases, the octahedron structure provides the closest match to the Boltzmann distribution, which is the expected distribution for a system in equilibrium. This finding confirms that the octahedron structure represents the most energetically favorable configuration under conditions of high entropy.

Shannon entropy

Shannon entropy serves as a metric for gauging the level of uncertainty or informational content contained within a dataset. Information theory enables the quantification of the average information necessary to describe or forecast an event. In the context of neural activity and the concept of equivalence classes, Shannon entropy offers valuable insights into the variability and diversity of neural responses. The resultant Shannon entropy value symbolizes the average level of information or uncertainty linked to the equivalence classes of neural activity. Higher entropy values signify an elevated degree of diversity and variation among these classes, whereas lower entropy values imply more predictable or uniform patterns.

In our model, we employ the computation of Shannon entropy to evaluate the interspike train activity of equivalence classes and compare it with the entropy associated with the network. As for Boltzmann entropy, we consider the equivalence classes determined by the ”mMd” criterion. The interspike train of each neuron within an equivalence class is analyzed to estimate its interspike activity, reflecting a temporal simulation of the class. Subsequently, the probability distribution of the equivalence classes is calculated by normalizing the data points attributed to each class with the interspike activity of the entire network denoted as *Nt*. Using the probabilities derived in the preceding step, we calculate the Shannon entropy of the network, as expressed in equation (1.3.7). Here, $p([n^i_{in}])$ represents the probability of each equivalence class, and the summation encompasses all equivalence classes. Each component of this sum, $-(p([n^i_{in}]) \times log_2(p([n^i_{in}])))$, is regarded as the entropy of the corresponding equivalence class.

Figures 2.5, 2.6, and 2.7 illustrate the Shannon entropy outcomes associated with equivalence classes and the activity of the neural network. Figure 2.5 illustrates the entropy distribution of the octahedrons and aligns with the Boltzmann entropy of equivalence classes. Notably, the equivalence class $[n^8_{12}]$, featuring the highest Boltzmann entropy value, also exhibits the highest Shannon entropy value, indicating a high degree of diversity and variability among the classes. Conversely, lower entropy values suggest more predictable or uniform patterns. Figure 2.6 presents the average network entropy value for a central delay of 20 ms across 20 simulations, with noise varying from 0 to 20 ms. In Figure 2.7, we examine the relationship between the average Shannon entropy of the network and the average interspike network activity. In this simulation, the central delay varies from 10 ms to 90 ms, and for each ”cd,” the noise varies from

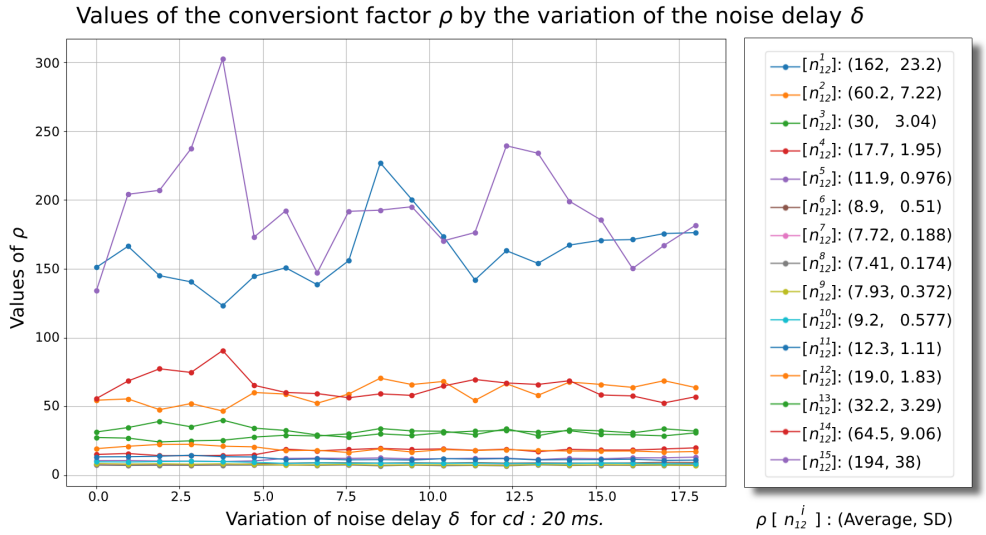

Figure 2.8: Brain neural heterogeneity, **H**. Keeping the parameters of the network in figure 2.2, the plot depicts the values of ρ for each octahedron $[n_{12}^i]$ $(1 \leq i \leq 15)$ by varying the noise delay δ in 20 steps from 0 to 20 ms for a *cd*= 20 ms.
The value of ρ represents the ratio between the total number of spikes of the network and the total number of spikes of the class $[n_{12}^i]$. We can notice how the ratio remains quite constant for those octahedrons close to the class with the highest entropy $[n_{12}^8]$.

0 to 20 ms. When dealing with systems characterized by spikes, each spike represents a specific outcome or state. A reduction in the number of spikes indicates a decrease in system diversity and the likelihood of certain outcomes. Consequently, the system becomes more predictable, and entropy decreases proportionally. High entropy values signify increased variability, while low entropy values indicate more predictable or uniform patterns. Consequently, the selection of equivalence classes and grouping criteria must be made judiciously to ensure the capture of desired data patterns.

Conversion factor ρ.

Furthermore, we report the ratio ρ between the number of spikes of *Nt* and its macrostate, as in 2.2. In figure 2.8 (neural heterogeneity), we plot the value of ρ for each octahedron of figure 2.2 as the value of noise increases from 0 to 20 ms, with a *cd*= 20 ms. We can notice how the closer we get to the octahedron at the highest entropy, $[n_{12}^8]$, the value of ρ tends to be constant while fluctuating for those far from it. The macrostates at higher entropy, therefore, offer a reasonable approximation of network spiking activity when axonal heterogeneity (noise) and neural heterogeneity are taken into account. This is because macrostates at high entropy are more stable, meaning fluctuations in neuronal activity due to heterogeneity and noise are minimized. The macrostates at higher entropy more accurately reflect the network's spiking activity.

General Discussion and Conclusion

We constructed three different model networks framed on a toroidal grid in multiple dimensions. This realization helps to mimic realistic brain patches where formal limits and edges are not defined, constraining data traffic in borderless areas. In the first part of the manuscript, we generalized what was found in previous studies related to the influence of heterogeneous axonal delay on various dimensions. This was to facilitate information transmission within a model neural network. We connect the initiator neuron n_{in} to an external current I, forcing it to regularly spike during the simulation time T and, consequently, to deliver signals to the adjacent nodes on the grid. The signal diffusion varies according to the grid structure, based on a von Neumann neighborhood model in 2D, 3D, and 4D dimensions. In all the simulations undertaken in this study, for all the three different dimensions of the network, the negative value of the regression line's slope *m*, figure 2.1, indicates how heterogeneous axonal delay (noise) induces faster propagation speed within the network. The robustness by which we find negative *m* as the studied models vary regarding dimensions and size, confirms the solidity of what we call the stochastic grid enhancement *SGE effect*. We extended the properties of this counter-intuitive result, generalizing the concept for any network dimension, showing that information contained in spikes travels faster under higher heterogeneous axonal delay randomness. Through an analytical demonstration and several simulations, we have shown that at any dimension the increase of heterogeneity, represented as a noise level in the axonal propagation delay, helps a signal (information) to spread within the network. Moreover, we investigated the role of neuron type heterogeneity in the same set of spiking neural networks. We did this by manipulating the parameters *c, d* of the Izhikevich model through a uniformly distributed random variable. The level of neural heterogeneity ranges from 0 to 1, with 0 representing a perfectly homogeneous regular spike (RS) neuron model network and 1 a heterogeneous one as defined in equations 1.2.1. In all cases, we set synaptic weights at $w = 18$, and the initiator neuron n_{in} input current at 10 mA.

Recognizably as shown in figures 2.9, by keeping constant the initial value of current, synaptic strength, and the number of neurons of the model, introducing cell type heterogeneity results in a large increase in firing activity a phenomenon that we called here stochastic neuron enhancement, *SNE effect*. The information created from the spiking activity was abundant in heterogeneous networks since the networks could increase spiking activity in the same period and with equal beginning values for the number of neurons, current, and synaptic strength. As a result, we conclude that the combination of axonal and neuronal heterogeneity is a metabolically efficient brain strategy. Heterogeneous networks have no additional cost in terms of neurons or synapses and outperform homogeneous networks with the same order of initial parameters. This neural cell heterogeneity is therefore a biologically and computationally effective strategy for the brain to improve signal robustness.

In addition, we introduced the concept of equivalent classes in a neural network, proving the minimum Manhattan distance (*mMd*) to be an equivalence relation on the network. Neurons are

considered equivalent if they have the same *mMd* from n_{in} neuron. These equivalent classes are referred to as octahedrons, and interspike trains are defined for each octahedron. The Boltzmann and Shannon entropy of the network are analyzed based on these equivalence classes, allowing for a higher-level understanding of the network's behavior and the identification of common optimization techniques. The theoretical model partitions the network into classes associated with their entropy, providing an alternative approach to evaluating network entropy and spike information. This partitioning helps calculate the entropy of each state and identifies the most probable state, optimizing computational performance by avoiding unnecessary calculations.

These findings contribute to understanding the fundamental characteristics of information transfer in the brain, providing a conceptual model for an explanation of other paradoxical phenomena in which neural heterogeneity and heterogeneous axonal delay appear to favor computational processes enhancing perception and other performance in human subjects. While in this study we kept parameter manipulation to a minimum to better clarify the effect of heterogeneity on information transmission. We also suggested further statistical analyses such as synchronization factors, discharge frequency, and other possible statistical analyses to deepen the understanding of spike information transmission.

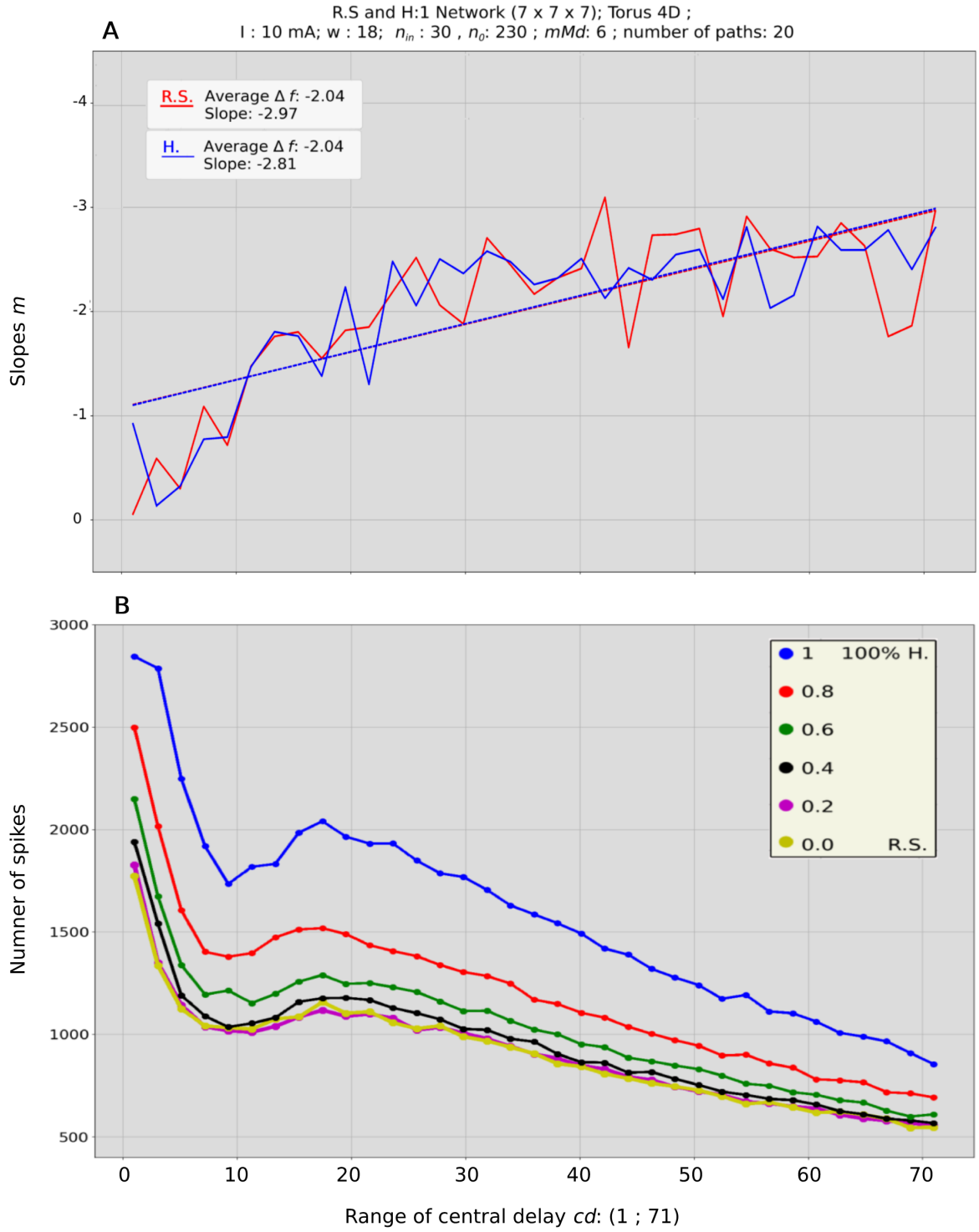

Figure 2.9:
A: A comparison of the SGE effect over two models of neural heterogeneity (H=1, blue) and a regular spiking model (H=0, R.S., red). According to panel **B**, the H=1 line shows the greatest amount of spiking activity, while the R.S. is the minimum. Nevertheless, the *SGE effect* acts similarly on both networks. All the models have the same constant current input of 10 mA, a synaptic strength of 18, and the same number of neurons. Noticeably, the heterogeneity offers the most suitable model regarding robustness (highest spiking activity) while keeping the benefit of improved spike propagation times (SGE effect).
B: The panel assesses the variations in spike counts at various central delays from 1 to 71 ms and across six different levels of heterogeneity. At each central delay value *cd*, the degree of randomness is adjusted in 15 incremental steps, as depicted in Figure 1.17. The total spike count is computed across all neurons in the network during the simulation period. Notably, when the neuronal heterogeneity is at its maximum, the model exhibits the most resilient spiking activity, which we refer to as the *SNE effect*

Compliance with Ethical Standards

Conflict of Interest: Marcello Salustri declares that he has no conflict of interest. Ruggero Micheletto declares that he has no conflict of interest.

Ethical approval: This article does not contain any studies with human participants performed by any of the authors.

List of Publications

Referred journals:

1. Salustri, Marcello and Micheletto, Ruggero, "Heterogeneous Axonal Delay Improves the Spiking Activity Propagation on a Toroidal Network", *Cognitive Computation* (2022), Springer. https://doi.org/10.1007/s12559-022-10034-2.

2. Salustri Marcello and Yoshida Shunra and Micheletto Ruggero, "Neural and axonal heterogeneity improves information transmission", *Physica A: Statistical Mechanics and its Applications* (2023), Springer. https://doi.org/10.1016/j.physa.2023.128627.

Under submission:

1. Salustri, Marcello and Micheletto, Ruggero, 'Partitioning of entropy in equivalence classes.', *Cognitive Computation* (2023), Springer. .
   Submitted on July 31, 2023.

Papers communicated in referred journals:

1. Sun, Zhe and Cutsuridis, Vassilis and Caiafa, Cesar F. and Solé-Casals, Jordi, "Brain Simulation and Spiking Neural Networks", *Cognitive Computation* (2023), Springer. https://doi.org/10.1007/s12559-023-10156-1.

Bibliography

[1] J.F. Pagel and P. Kirshtein. Chapter six - neural networks: The hard and software logic. pages 83–92, 2017.

[2] A. Tavanaei, M. Ghodrati, S.R. Kheradpisheh, T. Masquelier, and M. Maida. Deep learning in spiking neural networks. *Neural Networks*, 111:47–63, 2019.

[3] S. Feng and S. Zheng. How can artificial neural networks approximate the brain? *Frontiers in Psychology*, 13, 2023.

[4] T. Hongwei, Z. Yifan, Quanzheng, R. Johanna, and S. T. van Dijken. Bioinspired multisensory neural network with crossmodal integration and recognition. *Nature Communications*, 12, 2021.

[5] E. Manuylovich, D. Argüello Ron, M. Kamalian-Kopae, and S. Turitsyn. Stochastic resonance neurons in artificial neural networks. 2022.

[6] M. Kawaguchi, H. Mino, and D. Durand. Stochastic resonance can enhance information transmission in neural networks. *IEEE transactions on bio-medical engineering*, 58:1950–8, 03 2011.

[7] S. Radhakrishnan, S.and Sebastian, A. Oberoi, D. Sarbashis, and D. Saptarshi. A biomimetic neural encoder for spiking neural network. *Nature Communication*, 12, 4 2021.

[8] M. D. McDonnell and D. Abbott. What is stochastic resonance? definitions, misconceptions, debates, and its relevance to biology. *PLoS computational biology*, 5, 4 2009.

[9] O. van der Groen, M. F. Tang, N. Wenderoth, and J. B. Mattingley. Stochastic resonance enhances the rate of evidence accumulation during combined brain stimulation and perceptual decision-making. *PLOS Computational Biology*, 14(7):1–17, 07 2018.

[10] Harikrishnan N.B. and Nithin Nagaraj. When noise meets chaos: Stochastic resonance in neurochaos learning. *Neural Networks*, 143:425–435, 2021.

[11] Huixia Liu, Lulu Lu, Yuan Zhu, Zhouchao Wei, and Ming Yi. Stochastic resonance: The response to envelope modulation signal for neural networks with different topologies. *Physica A: Statistical Mechanics and its Applications*, 607:128177, 2022.

[12] W.C. Stacey and D.M. Durand. Stochastic resonance in simulated and in vitro hippocampal ca1 cells. 1:364 vol.1–, 1999.

[13] F. A. Azevedo, L.R. Carvalho, L. T. Grinberg, J. M. Farfel, R. E. Ferretti, R. E. Leite, W. Jacob Filho, R. Lent, and S. Herculano-Houzel. Equal numbers of neuronal and nonneuronal cells make the human brain an isometrically scaled-up primate brain. *J. Comp. Neurol.*, 10(513):532–541, April 2009.

[14] AT. Winfree. The geometry of biological time. *New York: Springer*, 2001.

[15] C. Koch and G. Laurent. Complexity and the nervous system. *Science*, 284:96–98, 1999.

[16] S. G. Tewari, M.K. Gottipati, and V. Parpura. Mathematical modeling in neuroscience: Neuronal activity and its modulation by astrocytes. *Frontiers in Integrative Neuroscience*, 10, 2016.

[17] A. Aldo Faisal, Luc P. J. Selen, and Daniel M. Wolpert. Noise in the nervous system. *Nat Rev Neurosci*, 9, APR 2008.

[18] Z. Budrikis. Forty years of stochastic resonance. *Nature Reviews Physics.*, 3(771), 2021.

[19] WC. Stacey and DM. Durand. Stochastic resonance improves signal detection in hippocampal ca1 neurons. *J Neurophysiol*, 83(3), MAR 2000.

[20] N. Perez-Nieves, V.C.H. Leung, and P.L. Dragotti. Neural heterogeneity promotes robust learning. *Nat Commun*, 12(5791), October 2021.

[21] B. Moret and M. et al. Donato, R.and Nucci. Transcranial random noise stimulation (trns): a wide range of frequencies is needed for increasing cortical excitability. *Scientific Report*, 9, 2019.

[22] J. von Neumann. Probabilistic logics and the synthesis of reliable organisms from unreliable components. *Automata Studies.*, 34:43–99., 1956.

[23] Richard J. Gardner, E. Hermansen, M. Pachitariu, Y. Burak, N. Baas, Benjamin A. Dunn, M. Moser, and Edvard I. Moser. Toroidal topology of population activity in grid cells. *Nature*, 602, 2022.

[24] G. Tononi, A.R. McIntosh, D.P. Russell, and G.M. Edelman. Functional clustering: Identifying strongly interactive brain regions in neuroimaging data. *Neuroimage.*, 7:133–149, 1998.

[25] T.O. Sharpee, A.J. Calhoun, and S.H. Chalasani. Information theory of adaptation in neurons, behavior, and mood. *Curr. Opin. Neurobiol.*, 25(25):47–53, 2014.

[26] Z. Huang, J. Zhang, J. Wu, G.A. Mashour, and A.G. Hudetz. Temporal circuit of macroscale dynamic brain activity supports human consciousness. *Sci. Adv.*, 6(eaat0087), 2020.

[27] A. Demertzi, E. Tagliazucchi, S. Dehaene, G. Deco, P. Barttfeld, F. Raimondo, C. Martial, D. Fernández-Espejo, B. Rohaut, H.U. Voss, and et al. Human consciousness is supported by dynamic complex patterns of brain signal coordination. *Sci. Adv.*, 5(eaat7603), 2019.

[28] CJ. Schwiening. A brief historical perspective: Hodgkin and huxley. *J Physiol.*, 590(11), 2012.

[29] E.M. Izhikevich. Simple model of spiking neurons. *IEEE Transactions on neural networks*, 14(6), 2003.

[30] Chang Wu, Yubai Li, and Song Chai. Design and simulation of a torus topology for network on chip. *Journal of Systems Engineering and Electronics*, 19(4):694–701, NOV 2008.

[31] J. Eppler, M. Helias, E. Muller, M. Diesmann, and M.-O. Gewaltig. Pynest: a convenient interface to the nest simulator. *Frontiers in Neuroinformatics*, 2(3), 2009.

[32] MO. Gewaltig, A. Morrison, and Plesser H.E. Nest by example: An introduction to the neural simulation tool nest. *Computational Systems Neurobiology*, pages 533–558, 2012.

[33] Soni Chaturvedi. Comparison of lif and izhikevich spiking neural models for recognition of uppercase and lowercase english characters. *CiiT International Journal of Digital Image Processing*, 6, 07 2014.

[34] S. Nobukawa, H. Nishimura, and T. Yamanishi. The importance of neighborhood scheme selection in agent-based tumor growth modeling. *Scientific Reports*, 8, 2018.

[35] L. Fang, N. Zhao, L. Caudal, H. Chang, R. Zhao, C. Lin, N. Hainz, C. Meier, B. Bettler, W. Huang, A. Scheller, F. Kirchhoff, and X. Bai. Impaired bidirectional communication between interneurons and oligodendrocyte precursor cells affects social cognitive behavior. *Nature Communications*, 13, 2022.

[36] M. Coli, P. Palazzari, and R. Rughi. The toroidal neural networks. *2000 IEEE International Symposium on Circuits and Systems (ISCAS)*, 4:137–140 vol.4, 2000.

[37] R. Suwanda, Z. Syahputra, and E. M. Zamzami. Analysis of euclidean distance and manhattan distance in the k-means algorithm for variations number of centroid k. *Journal of Physics*, 1566:696, NOV 2019.

[38] A. Schneider and M. Hommel, G.and Blettner. Linear regression analysis: part 14 of a series on evaluation of scientific publications. *Deutsches Arzteblatt international*, 107(44):776–782., 2010.

[39] SM. Chrysafides, S. Bordes, and S. Sharma. Physiology, resting potential. *NCBI National Center for Biotechnology*, 2021.

[40] Stephanie B. Aldrich. The use of multiple neurotransmitters at synapses. *Synaptic Transmission*, pages 449–480, 2019.

[41] A. Tozzi and F Peters. James. Towards a fourth spatial dimension of brain activity. *Cognitive neurodynamics*, 10(3), 2016.

[42] B. Sonal and G. Mahendra. Design of mesh and torus topologies for network-on-chip application. *International Journal of Reconfigurable and Embedded Systems (IJRES)*, 2, 07 2013.

[43] D. A. Zaitsev. A generalized neighborhood for cellular automata. *Theoretical Computer Science*, 666:21–35, 2017.

[44] M. Madadi Asl, A. Valizadeh, and P. Tass. Dendritic and axonal propagation delays determine emergent structures of neuronal networks with plastic synapses. *Scientific Report*, 7, 2017.

[45] M. Salustri and R. Micheletto. Heterogeneous axonal delay improves the spiking activity propagation on a toroidal network. *Cogn Comput*, June 2022.

[46] M. Sato and T. Sado. Lattice paths restricted by two parallel hyperplanes. *Bulletin of informatics and cybernetics*, 21(3/4):97–105, 1985.

[47] T. Britz, M. Mainetti, and L. Pezzoli. Some operations on the family of equivalence relations. *Springer Milano*, 1 2001.

[48] O. Ore. Theory of equivalence relations. *Duke Mathematical Journal*, 9(3):573 – 627, 1942.

[49] C. Cercignani. The boltzmann equation. *Springer New York*, 40(103):279–300, 1988.

[50] K. Uchiyama. A fluctuation problem associated with the boltzmann equation for a gas of molecules with a cutoff potential. *Japanese journal of mathematics. New series*, 9(1):27–53, 1983.

[51] Yeliz Karaca and Majaz Moonis. Chapter 14 - shannon entropy-based complexity quantification of nonlinear stochastic process: diagnostic and predictive spatiotemporal uncertainty of multiple sclerosis subgroups. pages 231–245, 2022.

[52] P. Županović and D. Kuić. Relation between boltzmann and gibbs entropy and example with multinomial distribution. *Journal of Physics Communications*, 2(4):045002, apr 2018.

[53] Alejandro A. Torres-García, Omar Mendoza-Montoya, Marta Molinas, Javier M. Antelis, Luis A. Moctezuma, and Tonatiuh Hernández-Del-Toro. Chapter 4 - pre-processing and feature extraction. pages 59–91, 2022.

[54] H. Nakahama, M. Yamamoto, K. Aya, K.vand Shima, and H. Fujii. Markov dependency based on shannon's entropy and its application to neural spike trains. *IEEE Transactions on Systems, Man, and Cybernetics*, SMC-13(5):692–701, 1983.

ACKNOWLEDGMENTS

It is a great pleasure for me to express my respect and a deep sense of gratitude to my supervisor Professor Micheletto Ruggero, Department of Physics Nanoscience College, Kanazawa-Hakkei, Yokohama City University, for his wisdom, vision, expertise, guidance, enthusiastic involvement and persistent encouragement during the planning and development of this research work. I also gratefully acknowledge his painstaking efforts in thoroughly going through and improving the manuscripts without which this work could not have been completed.

I am highly obliged to all members of the Faculty of Science of Yokohama City University, for providing all the facilities, help, and encouragement for carrying out the research work.

I am obliged to my parents Salustri Mario and Fondi Ecle for their moral support, love, encouragement, and blessings to complete this task. I am especially thankful to my wife Sato Marina, my daughters Arianna and Sofia, and my son Leo for her patience, love, and encouragement during this journey.

I also would like to express my deep and sincere thanks to my friends and all other persons whose names do not appear here, for helping me either directly or indirectly in all even and odd times.

I am also thankful to the anonymous reviewers of my research publications. Their comments and suggestions were very helpful in shaping my research work.

Salustri Marcello